Heliyon 10 (2024) e24098

Contents lists available at ScienceDirect

Heliyon

journal homepage: www.cell.com/heliyon

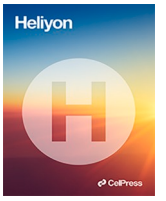

Research article

Numerical modeling of a MHD non-linear radiative Maxwell nano fluid with activation energy

Fariha Ahmed [a], Sk Reza-E-Rabbi [a,*], Md Yousuf Ali [b], Lasker Ershad Ali [a], Ariful Islam [a], Md Azizur Rahman [a], Raju Roy [a], Md Rafiqul Islam [c], Sarder Firoz Ahmmed [a]

[a] *Mathematics Discipline, Khulna University, Khulna, 9208, Bangladesh*
[b] *Department of Software Engineering, Daffodil International University, Dhaka, 1216, Bangladesh*
[c] *Department of Mathematics, Pabna University of Science and Technology, Pabna, 6600, Bangladesh*

ARTICLE INFO

Keywords:
Maxwell fluid
Nanofluid
EFD
Activation energy
Non-linear radiation
MHD

ABSTRACT

The present research explores linear as well as nonlinear radiation patterns based on the MHD non-Newtonian (Maxwell) nanofluid flow having Arrhenius activation energy. This study's core focus is MHD properties in non-Newtonian fluid dynamics and boundary layer phenomena analysis. It initiates with time-dependent equations, employing boundary layer approximations. Extensive numerical computations, executed with custom Compact Visual Fortran code and the EFD method, provide profound insights into non-Newtonian fluid behavior, revealing intricate force interactions and fluid patterns. To check the stability of the solution, a convergence and stability analysis is performed. With the values of $\Delta Y = 0.25$, $\Delta\tau = 0.0005$, and $\Delta X = 0.20$; it is found that the model convergence occurs to the Lewis number, $Le > 0.016$ as well as the Prandtl number, $Pr > 0.08$. In this context, investigating non-dimensional results that depend on multiple physical factors. Explanation and visual representations of the effects of different physical characteristics and their resultant temperatures, concentrations, and velocity profiles are provided. As a result of the illustrations, the skin friction coefficient and Sherwood number, which are calculated, as well as Nusselt values, have all come up in discussion. Additionally, detailed representations of isothermal lines and streamlines are implemented, and it is pointed out that the development of these features occurs at the same time as Brownian motion. Furthermore, the temperature field for Maxwell fluid is modified due to the impression of chemical reaction as well as the Dufour number (*Kr* and *Du*). Our research demonstrates the superior performance of non-Newtonian solutions, notably in cases involving activation energy and nonlinear radiation. This paradigm shift carries significant implications. In another context, the interplay between Maxwell fluid and nonlinear radiation is notably affected by activation energy, offering promising applications in fields like medicine and industry, particularly in groundbreaking cancer treatment approaches.

* Corresponding author.
E-mail addresses: fariha.ahmed1717@gmail.com (F. Ahmed), rabbi06@math.ku.ac.bd (S. Reza-E-Rabbi), yousufkumath@gmail.com (M.Y. Ali), ershad@math.ku.ac.bd (L.E. Ali), arif@math.ku.ac.bd (A. Islam), mdazizur@math.ku.ac.bd (M.A. Rahman), rajuroy@math.ku.ac.bd (R. Roy), rafiqku.islam@pust.ac.bd, rafiqku.islam@gmail.com (M.R. Islam), sfahmmed@math.ku.ac.bd (S.F. Ahmmed).

https://doi.org/10.1016/j.heliyon.2024.e24098
Received 12 July 2023; Received in revised form 17 December 2023; Accepted 3 January 2024
Available online 4 January 2024

Nomenclature

Variables

A	Linear stretching constants, [s^{-1}]
B	Magnetic component, [Wbm^{-2}]
C^*	Dimensional concentration, [mol m^{-3}]
C	Dimensionless concentration, [−]
c_p	Specific heat, [$Jkg^{-1}K^{-1}$]
C_w	Concentration at the surface, [mol m^{-3}]
C_∞	Concentration away from the surface, [mol m^{-3}]
D_B	Coefficient of Brownian diffusion, [−]
D_T	Coefficient of thermophoresis diffusion, [−]
g	Gravitational acceleration, [ms^{-2}]
k	Thermal conductivity, [$Wm^{-1}K^{-1}$]
κ	Boltzmann constant $1.3805 \times 10^{-23} JK^{-1}$
q_r	Radiative heat flux, [kgm^{-2}]
t	Dimensional time, [s]
T	Fluid temperature, [K]
T_w	Temperature at the surface
T_∞	Temperature away from the surface
u	Velocity component in x direction, [ms^{-1}]
U	Non-dimensional velocity component, [−]
U_w	Uniform velocity, [ms^{-1}]
v	Velocity component in y direction, [ms^{-1}]
V	Non-dimensional velocity component, [−]
V_w	Uniform velocity, [ms^{-1}]
x	Cartesian x coordinate
X	Non-dimensional x coordinate
y	Cartesian y coordinate
Y	Non-dimensional y coordinate

Parameters and Numbers

AE	Activation energy parameter, [−]
Cf	Skin friction coefficient, [−]
Du	Dufour number, [−]
Ec	Eckert number, [−]
Gr	Thermal Grashof number, [−]
Gm	Mass Grashof number, [−]
Kr	Chemical reaction parameter, [−]
Le	Lewis number, [−]
M	Magnetic parameter, [−]
Nb	Brownian parameter, [−]
Nt	Thermophoresis parameter, [−]
Nu	Nusselt number, [−]
Nv	Maxwell parameter, [−]
Pr	Prandtl number, [−]
Ra	Radiation parameter, [−]
Sh	Sherwood number, [−]

Greek Symbols

β_C	Mass distribution coefficient
β_T	Heat distribution coefficient
γ	Temperature related parameter
λ	Relaxation time effect, [s]
υ	Kinematic viscosity, [m^2s^{-1}]
τ	Dimensionless time
ρ	Fluid density, [kgm^{-3}]
σ	Stefan-Boltzmann constant
θ	Non-dimensional temperature
θ_w	Temperature differences

*Abbreviations

EFD	Explicit Finite Difference
MHD	Magneto-hydrodynamics
PDE	Partial Differential Equation

1. Introduction

Non-Newtonian fluids defy Newton's viscosity law, altering viscosity under force. For instance, ketchup thickens when agitated. These fluids find extensive use in engineering, applied science, and industry. Conventional fluid models fall short in representing the complexity of non-Newtonian fluids. This resulted in various academics referencing numerous models at various times [1,2]. Zhu et al. [3] mentioned earlier in their experiment that combining starch and polymer alters the viscosity peak to a higher frequency, allowing for high-speed polishing. Extensional viscosity has been previously observed by Finotello et al. [4] to have an influence on a fluid which is non-Newtonian with a given shear-thinning, where the viscosity is no longer constant throughout contact. Nonetheless, it is demonstrated that the Weber number (*We*), which has no dimensions and impact factor (*B*) predominate and distinguished between Newtonian and non-Newtonian fluids. Additionally, a comprehensive investigation demonstrated that greater viscosity dispersal of energy and extensional consequences are to blame for this outcome. Several academics continue to assess diverse effects and impacts from various vantage points.

The creation of nanofluids, achieved by blending base fluids with minute metal nanoparticles, represents a remarkable scientific innovation. Common base fluids include water, oil, and ethylene glycol. Nanofluids hold great significance in heat transfer due to their exceptional properties. They have a higher coefficient of convective heat movement and better thermal conductivity than the basal fluid. Pordanjani et al. [5] emphasized that nano fluids typically exhibit superior heat transfer capability in energy systems compared to purified fluids because of it is employed with a metal oxide particle combination, while studies of performance have demonstrated that nano fluids are appropriate for usage in applications in industry. Using nano fluids also reduces the number of resources used, waste created, materials used, and harm done to the environment. However, Ramezanizadeh et al. [6] showed that understanding the rheological behavior of nanofluids is essential for determining whether or not they are acceptable for convective heat transfer applications as far as the thermal act of nanofluidic thermosyphons is extensively affected by the type of nanoparticles used. Moreover, the ability of small nanoparticle concentration to enhance heat and mass transport was established in tests by Ahmadi et al. [7] upon the thermal conduction of multiple nanofluids because of Brownian motion increases as temperature rises, thermal conductivity also rises. In addition, Maxwell did not enter the field as a consequence of his research into eccentric viscosity or eccentric springs, to return to the topic that made him famous, Maxwell fluids. In extensive studies dating back to 1866, he examined the properties of gases and fluids in general. Puri et al. [8] demonstrated that the term "non-Newtonian fluids" refers to a wide variety of liquids with rheological properties, such as paints, cosmetics and shampoo, lubricants, specific oils, blood, toiletries, preserves, melted butter, jellies, mud, and detergent. Non-Newtonian fluid models are often classified as differential, rate, or integral, as mentioned by Fetecau et al. [9] in a prior study. Maxwell fluids, a form of rate-type fluids, can explain the process of relaxation. Moreover, it is reasonable to anticipate precise results from Maxwell fluid. A mathematical investigation of the mass along with heat transmission in a Maxwell fluid was carried out by Khan et al. [10]. It is also demonstrated that the characteristics of thermal stratification and concentration stratification effect on temperature as well as concentration distribution. Farooq et al. [11] used BVPh 2.0 to investigate the motion of the MHD effect of Maxwell liquid on a surface that was extending in an exponential way. Fetecau et al. [12] observed the mathematical analysis of non-Newtonian (Maxwell) fluid flow that accounted for the porous effect, and the results showed that a porous medium delays steady state. Hayat et al. [13] explored the ferromagnetic impact of a Maxwell fluid movement adopting the discharge method. It is shown that velocity and concentration profiles significantly improve when elastic as well as thermophoresis variables are modified. In addition, Hosseinzadeh et al. [14] conducted experiments on a Maxwell fluid with a chemically radiative flow, taking nonlinear radiation into account and concentrating on the direct impact of rise in Prandtl number on temperature and the Nusselt number. The Runge-Kutta technique was used by Shehzad et al. [15] to demonstrate how spontaneous convective Maxwell circulatory of fluid impacts a spinning disc that swings as a result of thermophoretic activity. Furthermore, Reza-E-Rabbi et al. [16] inspected that the presence of nano-sized particles in Maxwell fluids affects the temperature field of Casson fluid in their experiment. Some variables (*Nt, Pr,Nb, Du, Le,* and *Sr)* affect the fields of both fluids. One of the noteworthy outcomes is temperature profiles rise due to a surge of thermophoresis and Brownian parameter, whereas they decline due to an improvement of Casson fluid parameter.

Magnetohydrodynamics (MHD) studies electrically conducting fluids like salt water, liquid metals, and plasmas. This field, initiated by Alfvén's Nobel Prize-winning work, explores how magnetic fields influence fluid motion and induce electromagnetic-hydrodynamic waves [17]. Hussain et al. [18] presented an optimized model in which the magnetic field was decreased in response to a rise in perturbation caused by an upsurge in Hartmann number and a few waves number as a consequence of previous MHD research establishing an important fact. In addition, it has been reported that the flow becomes unstable when Re grows due to an increase in growth rate. In a previous study by Chen et al. [19], it has been looked at flow in the boundary layer of a viscoelastic MHD fluid across a extending sheet and came to the conclusion that the stronger the elastic characteristic, the more oscillating the phenomenon, and the lower the strain parameter, the more viscous the behavior. In accordance with Khan and others [20], with the appearance of the Dufour, chemical reaction and Soret effect, which converts a nonlinear differential system into a linear one by utilizing a similarity variable, MHD convective flow was seen across a spinning cone. Jabeen et al. and Noor [21,22] used radiation, thermophoresis, as well as chemical reaction to investigate the flow of MHD around a stretchable plate. Maxwell fluid has a greater capacity of heat and mass transport than Newtonian fluids and some other non-Newtonian liquids, according to Jabeen et al.'s

observations, it is pointed out that the thickness of the mass boundary layer decreases for Maxwell fluid, the values of Schmidt number, thermophoresis, chemical reaction factor, and Schmidt number increases. Akinshilo [23] investigated the effects of the radiative parameter, pressure gradient, Reynolds number, and magnetic Prandtl number on an MHD fluid flow, and a Runge-Kutta numerical solution of the fourth order supported the agreement. Henceforth, the increased radiation parameter results in a decrease in temperature distribution, which has an impact on the electrically conducting wall. This is a noteworthy finding from the observation. In a recent study, Chabani et al. [24] utilized COMSOL to analyze the effects of Cu–TiO_2 as an integrated nano fluid in a triangular field with a meandering obstacle using the Darcy-Brinkman-Forchheimer model and concluded that triangular obstructions can enhance thermal transfer, which is a major finding. Whereas, Reza-E-Rabbit et al. [25] utilized the explicit finite difference methodology and Compact Visual Fortran to examine the uneven MHD flow of Casson fluid in order to measure the impression of thermal radiation as well as chemical processes. A substantial comparison line between Maxwell and Casson fluid has been made, showing that the thermal and mass properties greatly improve, supporting earlier findings. Temperature rises with thermal relaxation and radiation parameter, as Kumar et al. [26] showed in their numerical investigation of MHD micropolar fluid using a modified flux model. Recent research conducted by Lou et al. [27] on a dual phase dusty MHD micropolar liquid that was subject to Lorentz and Coriolis forces revealed that the Nusselt number decreased as rotation, material factor, and dust element volume concentration increased.

Our flow model incorporates heat radiation, vital in mixed convective flow with hydromagnetic effects. It finds applications in heat exchangers, gas turbines, combustion chambers, nuclear plants, steel forging, metal extraction, and glass production, prompting increased research on thermal radiation. Crane [28] studied boundary layer flow over a stretching surface. Understanding radiation's impact on heat transfer is crucial across industries, especially at high temperatures, where fluid temperature profiles and heat transmission rates vary significantly. Research covers both linear and nonlinear radiation, with emphasis on boundary conditions with linear temperature fluctuations. Ghadikolaei et al. [29] explored the paraphernalia of nonlinear radiation while conducting an experiment with Casson fluid over a porous medium positioned at an incline. They demonstrated that the presence of Lorentz drag reduces fluid flow velocity by increasing the Hartman number and Casson fluid parameter. Using the RKF-45 method of numerical analysis, Gireesha et al. [30] also investigated the impact over the Jeffrey fluid in three dimensions. The research established that precise boundaries for the space- and temperature-dependent production or absorption of heat. Using Maxwell fluid, Ahmed et al. [31] investigated transmission characteristics the mass and heat of nanofluid in the survival of a magnetic field induced by a stretching cylinder. Chu et al. [32] studied nonlinear thermal radiation aspects of heat generation and absorption in nanofluids containing gyrotactic microorganisms comprising rate-type nanofluids. The authors' key finding was that the heat transmission of the nanofluid has been significantly increased by the thermophoresis parameter, radiation parameter, Brownian motion constant, and surface heating parameter In a recent study, Gautam et al. [33] hypothesized a comparison of the nonlinear thermal radiation impact between bio-convective MHD Casson and Maxwell nanofluid, and the results demonstrated that the velocity of Casson fluid was significantly more dominant than Maxwell fluid. In a previous study, Ali et al. [34] demonstrated that for an MHD flow, both radiation and thermoelectric improve the heat transmission capability. One significant conclusion of the study reveals that the amount of Nanofluid flow declines as thermal radiation rises.

Various scientific domains, including chemical engineering, food processing, geothermal resources, and oil emulsions, address mass transfer due to chemical reactions and activation energy. When different species' concentrations change during a reaction, mass transfer occurs. Activation energy (AE) is the energy threshold for a specific reaction. Concentrations shift as reactions proceed. Logan's work explores the origins and significance of the Arrhenius equation, a vital tool for understanding chemical kinetics. Moreover, the research employs the Buongiorno model theory [35] to integrate thermophoretic and Brownian dispersion. According to Rafiq et al. [36], activation energy augments the concentration profile of a fluid. The authors delve into the extensive research field that is activation energy. Zhang et al. [37] conducted experiments investigating the radiation as well as activation energy impacts of Maxwell fluid over a stretching plate. Khan et al. [38] also reported the influence of activation energy on linear thermal radiative Walter-B nanofluid. In addition, it is also found that a connection between the temperature profile, the activation energy, and the Weissenburg number. Researchers [39] presented a novel chemical species model that addressed the energy of the Darcy-Forchheimer nanomaterial flow through an impermeable cylinder and explained the effect of activation energy. Furthermore, Salawu et al. [40] discovered that, when using Maxwell nanofluid, activation energy research is crucial to the propagation of dual chemical mixes of energy as species transport, which will help chemical engineers and others avoid reaction blowup. Alsaadi et al. [41] examined the effect of nonlinear radiative heat flux utilizing Williamson fluid across a heated stretchable sheet. Additionally, Brownian diffusion has been incorporated into the mathematical model's structure. The fluctuations of activation energy on Carneau fluid were discovered by Ijaz Khan and his peers [42]. The investigation utilized the discharge method, Brownian diffusion, and thermophoresis. The dominance of nonlinear thermal radiation as well as activation energy of Casson fluid is previously explored by Reza-E-Rabbit et al. [43]. Additionally, it is found that the role of magnetism in controlling heat transport. Whereas author's significant finding nder the influence of activation energy it is observed that nonlinear radiation had a considerable impact on the mass transmission down the wall, revealing the fluid's substantial action relative to a Newtonian one motivates the current study. Therefore, Li et al.'s recent study [44] examined the impact of activation energy together with chemical reaction on the magnetohydrodynamic (MHD) fluid flow caused by the compression of Casson by Darcy-Forchheimer via porous media in a horizontal channel. As the thermal relaxation parameter increases, the temperature dynamics of the hybrid Williamson nanofluid mixture show a declining trend. Meanwhile, an increase in the Weissenberg number leads to an augmentation in the density of microorganisms and concentration profiles within the fluid domain. Sreedevi et al. [45], using the similarity transformation method, shed light on the complex interplay of variables in this intricate system. Employing the finite element method, Chandra Sekar Reddy [46] confirmed that an increase in the nanoparticle volume fraction enhances the velocity of the hybrid nanofluid. Moreover, it was observed that the temperature of the hybrid nanofluid rises with increasing Biot number values. Reddy et al. [47] explored the influence of an updated Fourier's heat flux on thermal transport in a

Table 1
Comparison with previous work based on literature review analysis.

Authors	NNF	LR	NLR	NF	AAE
Reza-E-Rabbi et al. [43]	✓	✓	×	✓	×
Ijaz et al. [42]	✓	×	✓	✓	×
Alsaadi et al. [41]	✓	×	×	✓	✓
Salawu et al. [40]	✓	×	×	✓	✓
Khan et al. [39]	✓	×	×	✓	✓
Rafiq et al. [36]	✓	×	×	✓	✓
Chu et al. [32]	✓	×	✓	✓	×
Ahmed et al. [31]	✓	×	✓	✓	×
Present work	✓	✓	✓	✓	✓

*Abbreviation: NF-nanofluid; NNF-non-Newtonian fluid; LR-linear radiation; NLR-nonlinear radiation; AAE-Arrhenius activation energy.

hybrid nanoliquid. Their Galerkin finite element study found that adding 0.03 vol fraction of magnesium oxide nanoparticles boosts heat transfer by 4.2 %–15.8 %. In another work [48], the authors investigated temperature and concentration effects on heat and mass transmission in a Maxwell hybrid nanofluid. They transformed equations using similarity reductions, showing that rising thermal relaxation parameter values decrease temperature fluctuations. The finite element method was employed to solve these equations. Additionally, Reddy et al. [49] analyzed heat and mass transfer in a hybrid nanoliquid flow over a stretching or shrinking surface, accounting for factors like chemical reactions, suction, slip effects, and thermal radiation. Their research revealed that an increased volume fraction of nanoparticles raises the temperature of the hybrid nanoliquid in both unsteady and steady scenarios. It is also found in another work [50] by introducing single-walled carbon nanotubes at a volume fraction of 0.05 in the base fluid increases the heat transfer rate by 6.2 %–15.6 %. Santhi et al. [51] used the finite element approach and observed that as the volume fraction of both nanoparticles increases, the temperature of the hybrid nanoliquid rises in both stable and unstable scenarios. Furthermore, Prabhavathi et al. [52], employing the variational finite element method, provided a numerical solution for the magnetohydrodynamic (MHD) boundary layer heat and mass transfer in nanofluids over a vertical cone saturated by a porous medium. They focused on Al2O3-water and Cu-water-based nanofluids with volume fractions of 1 % and 4 %. In their study, Zeeshan et al. [53] explored the magnetohydrodynamic transport of Casson nanofluid flow around a porous stretching cylinder, finding that as the chemical reaction parameter increased, the nanoparticle concentration distributions decreased, exhibiting a divergent pattern in comparison to the activation energy parameter. Arain et al. [54] investigated the unsteady flow in rotating circular plates containing Reiner-Rivlin nanofluid situated at a finite distance, revealing that as the Peclet number values increased, the microorganism profile decreased, whereas an increase in the bioconvection number led to a rise in the microorganism profile. In their experiment, Ali et al. [55] examined the flow of a two-dimensional non-Newtonian Oldroyd-B fluid through the upper horizontal paraboloid surface (UHPS) and found that increasing the paraboloid surface thickness parameter decreased the local skin friction coefficient.

The current work was motivated by earlier scholarly attempts to understand how activation energy affects time-dependent emission Maxwell nano fluid motion on a stretched sheet. Reza-E-Rabbi et al.'s work [25] has undergone rigorous analysis, but the proposed study is elaborated on this work. Previously, the implications of temperature and mass parameters, as well as a comparison between Maxwell and Casson fluid, had been investigated; however, no research has been done on the impact of linear and nonlinear radiation. The current investigation will focus on the impacts of thermal radiation that is both linear and nonlinear, as well as the influence of activation energy on Maxwell fluid. Thermal radiation was the focus of this investigation due to its significant contribution to the advancement of cancer treatment. Thermal radiation, specifically nonlinear radiation, generates high temperatures and has a substantial effect on industrial processes and cancer treatment technology. At the beginning of every chemical reaction, activation energy is essential. To initiate a chemical reaction or to break a chemical bond, a minute amount of activation energy is required. This quality applies more to the chemical and pharmaceutical industries. Again, this extension is prompted by the incomplete nature of the authors' work, which prevents them from investigating Brownian diffusion, the thermophoresis parameter on the isotherm, and the streamline. In addition, the proposed study's analysis is based solely on Maxwell fluid, and its determination of activation energy is a completely original research endeavor. The detection of heat radiation for both linear and nonlinear patterns, as observed via graphical representation, will be one of the most important findings of this investigation. Furthermore, Table 1 represents the contrast of the present investigation with the earlier published works.

2. Applications

The influence and impact of heat radiation in both linear and nonlinear patterns as well as Arrhenius activation energy are the primary focus of this current investigation. As a result, the thermal radiation factor has the potential to be effective for both medical and industrial uses. The main aspects of industrial purposes are laser cutting, additive manufacturing, such as 3D paints, surface modification of materials, heat treatment of metals, and drying of materials where thermal radiation helps to soak the moisturizer and leaves it dry. These are just a handful of the regions that are most useful for industrial purposes. Additionally, hyperthermia therapy, which employs heat to treat cancer, has the potential to be used in medical settings, or more specifically in the treatment of cancer. High-intensity laser beams, a type of nonlinear radiation heat the tumor, thermally harming cancer cells and causes cell death. Additionally, carbon nanotubes can be employed to induce hyperthermia using nonlinear thermal radiation. The tumor is filled with carbon nanotubes, which are then heated by non-linear thermal radiation, such as infrared radiation, causing the tumor to become

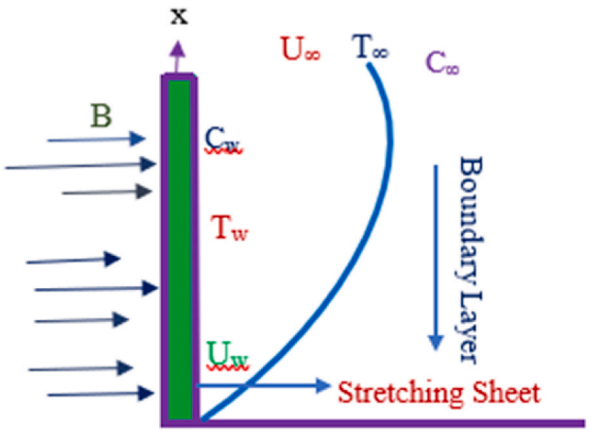

Fig. 1. Physical Configuration of the flow.

overheated. Also, the use of radiotherapy and thermo-radiotherapy assists in the treatment of cancer by destroying the DNA of cancer cells and preventing them from proliferating and regenerating new cells.

The primary application of Arrhenius activation energy is in the development of hyperthermia therapy, which is a key component of cancer treatment. Additionally, it is used in dosimetry, which counts the total amount of heat that a cancer cell has absorbed and monitors the temperature range at which cancer cells are most vulnerable to dying from heat-induced cell death during hyperthermia therapy. In drug formulation, stability testing, and drug development, Arrhenius activation energy is probably employed additively. Most likely plays vital role in food preservation. Numerous industrial processes use the Arrhenius activation energy, notably those involving chemical reactions and material deterioration. Some of these include the kinetics of chemical reactions, polymer breakdown, corrosion, and heat processing. Key industrial applications include laser cutting, additive manufacturing (including 3D printing), surface modification of materials, heat treatment of metals, and drying processes that utilize thermal radiation for moisture removal. These are among the primary settings suited for industrial use. Furthermore, hyperthermia therapy harnesses heat for medical purposes, particularly in cancer treatment. Nonlinear radiation, like high-intensity laser beams, is employed to raise tumor temperatures, causing thermal damage to cancer cells. This effect can also be achieved using carbon nanotubes within the tumor, which heat up through non-linear thermal radiation, such as infrared radiation, resulting in the overheating of the tumor.

3. Methodology

This continuing project uses numerical simulation for tracking the implication of linear together with nonlinear radiation in addition to the Arrhenius activation energy. In their earlier studies, Reza-E-Rabbi et al. [43] failed to observe heat radiation in a nonlinear pattern. Thus, new addition to the ongoing research is the measurement of the Arrhenius activation energy as well as heat radiation in nonlinear pattern. Since the entire project is built on numerical simulation, we used the EFD (Explicit Finite Difference) method to implement strategic stages to reach our goal. Meanwhile, while stability and converging tests are also done, the structure's overall accuracy improves. The following are a few steps that structure the entire work from beginning to end.

- The basic principle of fluid mechanics has been used to produce a set of fundamental equations such as continuity, diffusion balance, energy and momentum equations
- Because of the use of several types of dimensionless variables, the generated equations are dimensionless.
- Utilizing the EFD approach, the suggested equations are quantitatively resolved.
- A complete set of stability especially convergence requirements has been developed to guarantee that the solution converges.
- The numerical data is collected using the Visual Fortran software program, and by using the Tec plot software, the numerical data is evaluated and a graphical representation is created.
- Finally, in the section covering outcomes and discussion, the velocity, concentration, temperature, streamline, and isothermal profiles are shown, along with distinct flow fields. In addition, a brief comparison of Maxwell and non-Newtonian liquids has been presented. It has been investigated here how physically various parameters behave.

4. Mathematical analysis

On the behavior of unstable 2D incompressible non-Newtonian magnetized (MHD) motion of Maxwell liquid, the impact of nanoparticles, thermal radiation, and arousing energy impact were studied. Here, it is considered the fluid velocity and the stretching constant A. is the force that produces a magnetic area in the path of a fluid. When time (t) exceeds zero, the fluid's temperature T and concentration C increase both near to and far from the wall (Fig. 1).

4.1. Continuity equation

Due to the concept of mass conservation, the continuity equation for an incompressible fluid has the vector form $q\ (u, v)$, where v and u are the fluid's velocities. The Cartesian coordinate states that,

$$\frac{\partial v}{\partial y} = -\frac{\partial u}{\partial x} \tag{1}$$

4.2. Momentum equation

Newton's Second Law, which correlates a fluid component's acceleration or rate of shifting momentum to the total force acting on it, is reflected in the momentum equation. Momentum equation is another name for the Navier-Stokes equation for an incompressible fluid.

$$\frac{\partial q}{\partial t} = \upsilon \nabla^2 q - (q.\nabla)q + F - \frac{1}{\rho}\nabla p$$

Along with the Maxwell fluid term, the model has now considered buoyancy force and magnetic force, which are the body forces. As a result, the pressure gradient term becomes less accurate. In addition, the viscosity of Maxwell fluids produces. Now, by combining these and boundary layer estimations, the above-mentioned equation in the x direction becomes,

$$\frac{\partial u}{\partial t} + u\frac{\partial u}{\partial x} + v\frac{\partial u}{\partial y} = g\beta_T(T - T_\infty) - \frac{\sigma B^2 u}{\rho} + g\beta_C(C^* - C_\infty) - \alpha\left(u^2\frac{\partial^2 u}{\partial x^2} + 2uv\frac{\partial^2 u}{\partial x \partial y} + v^2\frac{\partial^2 u}{\partial y^2}\right) + \upsilon\frac{\partial^2 u}{\partial y^2} \tag{2}$$

The u and v values along the x and y axes here reflect the velocity components. Also, the impact of the relaxing period shown by α.

4.3. Energy equation

The energy equation precisely maintains the fluid's energy balance. The vector form of an incompressible nano fluid's energy equation is expressed as

$$\frac{\partial T}{\partial t} = \frac{1}{(\rho c_p)_f}\left[\nabla.(\kappa\nabla T) + (\nabla c.\nabla T)(\rho c_p)_p D_B + (\rho c_p)_p(\nabla T.\nabla T)\frac{D_B D_T}{T_\infty}\right] + \varphi$$

The viscous dissipation conception, the boundary layer estimation, and the heat radiation for the Maxwell nanofluid all modify the aforementioned equation, as shown below.

$$\frac{\partial T}{\partial t} = \frac{\kappa}{\rho C_P}\frac{\partial^2 T}{\partial y^2} - \left(u\frac{\partial T}{\partial x} + v\frac{\partial T}{\partial y}\right) + \lambda\left[D_B\left(\frac{\partial C}{\partial y}\frac{\partial T}{\partial y}\right) + \frac{D_T}{T_\infty}\left(\frac{\partial T}{\partial y}\right)^2\right] + \frac{D_m K_T}{C_S C_P}\frac{\partial^2 C^*}{\partial y^2} - \frac{1}{\rho C_P}\frac{\partial q_r}{\partial y} + \frac{\upsilon}{C_P}\left(\frac{\partial u}{\partial y}\right)^2$$

Here in the above equation, at constant pressure the specific heat has been obtained by C_p. Thermophoresis and Brownian diffusivity are respectively defined by D_B and D_T. κ represents the thermal conductivity. Besides, the Rosseland diffusion for radiative $q_r = -\frac{4\sigma'}{3k_s}\frac{\partial T^4}{\partial y}$ where, k_s stands for mean absorption coefficient. Alongside σ' is the Stefan Boltzmann constant. The nonlinear radiation term can be deducted as $-\frac{\partial q_r}{\partial y} = \frac{16\sigma'}{3k_s}\left(\left(\frac{\partial T}{\partial y}\right)^2 T^2 + T^3\frac{\partial^2 T}{\partial y^2}\right)$, now the equation turns into,

$$\frac{\partial T}{\partial t} + u\frac{\partial T}{\partial x} + v\frac{\partial T}{\partial y} = \frac{\kappa}{\rho C_P}\frac{\partial^2 T}{\partial y^2} + \lambda\left[\left(\frac{\partial T}{\partial y}\frac{\partial C^*}{\partial y}\right)D_B + \frac{D_T}{T_\infty}\left(\frac{\partial T}{\partial y}\right)^2\right] + \frac{D_m K_T}{C_S C_P}\frac{\partial^2 C^*}{\partial y^2} + \frac{1}{\rho C_P}\frac{16\sigma'}{3k_S}\left(T^3\frac{\partial^2 T}{\partial y^2} + T^2\left(\frac{\partial T}{\partial y}\right)^2\right) + \frac{\upsilon}{C_p}\left(\frac{\partial u}{\partial y}\right)^2 \tag{3}$$

4.4. Concentration equation

The concentric equation for the nano fluid is $\frac{\partial C^*}{\partial t} + q.\nabla C^* = \nabla D_T\frac{\nabla T}{T_\infty} + \nabla D_B\nabla C^*$

Now, using the boundary layer approximation theory in presence of activation energy concentric equation becomes

$$\frac{\partial C^*}{\partial t} = \frac{D_T}{T_\infty}\frac{\partial^2 T}{\partial y^2} - \left(u\frac{\partial C^*}{\partial x} + v\frac{\partial C^*}{\partial y}\right) + D_B\frac{\partial^2 C^*}{\partial y^2} - \sigma^2(C^* - C_\infty)^P\left(\frac{T}{T_\infty}\right)^n e^{\left(\frac{E_a}{KT}\right)} \tag{4}$$

Initial border circumstances included by

$$\begin{aligned} &t \le 0, C^* = C_\infty, u = Ax, T = T_\infty, v = 0 \vee x, y \\ &t > 0, T = T_\infty, u = 0, C^* = C_\infty, v = 0 \quad \text{for } x = 0 \\ &C^* = C_w, u = Ax = U_w, T = T_w, v = 0 \quad \text{for } y = 0 \\ &C^* \to C_\infty, u = 0, v = 0, T \to T_\infty, \text{as } y \to \infty \end{aligned} \tag{5}$$

Now the dimensionless variables are

$$U = \frac{u}{U_w}, V = \frac{v}{V_w}, X = \frac{xU_w}{\upsilon}, Y = \frac{yU_w}{\upsilon}, \tau = \frac{tU_w^2}{\upsilon}, \theta = \frac{T - T_\infty}{T_w - T_\infty}, C = \frac{C^* - C_\infty}{C_w - C_\infty}, \theta_w = \frac{T_w}{T_\infty} \tag{6}$$

now using the dimensionless variables from equation (6) and the non-dimensional parameters mentioned below, the above equations (1)–(5) have been converted to equations (7)–(11) as,

$$\frac{\partial U}{\partial X} + \frac{\partial V}{\partial Y} = 0 \tag{7}$$

$$\frac{\partial U}{\partial \tau} = Gr\theta + GmC - \left(V\frac{\partial U}{\partial Y} + U\frac{\partial U}{\partial X}\right) - Nv\left(V^2\frac{\partial^2 U}{\partial Y^2} + U^2\frac{\partial^2 U}{\partial X^2} + 2UV\frac{\partial^2 U}{\partial X \partial Y}\right) - MU + \frac{\partial^2 U}{\partial Y^2} \tag{8}$$

$$\begin{aligned} \frac{\partial \theta}{\partial \tau} = Pr^{-1}\left[1 + Ra\{1 + (\theta_w - 1)\theta\}^2\right]\frac{\partial^2 \theta}{\partial Y^2} - \left(U\frac{\partial \theta}{\partial X} + V\frac{\partial \theta}{\partial Y}\right) + Nb\left(\frac{\partial C}{\partial Y}\frac{\partial \theta}{\partial Y}\right) + Nt\left(\frac{\partial \theta}{\partial Y}\right)^2 \\ + Du\frac{\partial^2 C}{\partial Y^2} + Pr^{-1}\, Ra\{1 + (\theta_w - 1)\theta\}^2\left(\frac{\partial \theta}{\partial Y}\right)^2 + Ec\left(\frac{\partial U}{\partial Y}\right)^2 \end{aligned} \tag{9}$$

$$\frac{\partial C}{\partial \tau} + U\frac{\partial C}{\partial X} + V\frac{\partial C}{\partial Y} = Nt(NbLePr)^{-1}\frac{\partial^2 \theta}{\partial Y^2} + (LePr)^{-1}\frac{\partial^2 C}{\partial Y^2} - Kr(\gamma\theta + 1)^n e^{\left(\frac{-AE}{\vartheta\theta + 1}\right)} C \tag{10}$$

Additionally, the relevant boundary conditions are

$$\begin{aligned} &\tau \le 0, V = 0, C = 0, U = 0, \theta = 0 \quad \text{for all } X, Y \\ &\tau > 0, \theta = 0, V = 0, C = 0, U = 0, \text{for } X = 0 \\ &V = 0, C = 1, U = 1, \theta = 1, \text{for } Y = 0 \\ &\theta = 0, V = 0, C = 0, U = 0 \quad \text{as } Y \to \infty \end{aligned} \tag{11}$$

here the dimensionless parameters used as, Maxwell parameter, $Nv = \frac{\lambda U_w^2}{\upsilon}$; magnetic parameter, $M = \frac{\sigma B^2 \upsilon}{\rho U_w^2}$; thermophoresis parameter, $Nt = \frac{\lambda D_T (T_w - T_\infty)}{T_\infty \upsilon}$; thermal Grashof number, $Gr = \frac{g\beta_T (T_w - T_\infty)\upsilon}{U_w^3}$; mass Grashof number, $Gm = \frac{g\beta_C (C_w - C_\infty)\upsilon}{U_w^3}$; Brownian parameter, $Nb = \frac{\lambda D_B (C_w - C_\infty)}{\upsilon}$; Dufour number, $Du = \frac{D_m k_T}{C_s C_p \upsilon}$; Prandtl number, $Pr = \frac{\upsilon}{\alpha}$; radiation parameter, $Ra = \frac{16\sigma' T_\infty^3}{3k_S \lambda}$; Eckert number, $Ec = \frac{U_w^2}{C_P (T_w - T_\infty)}$; Lewis number, $Le = \frac{\alpha}{D_B}$; Arrhenius activation energy parameter, $AE = \frac{EA}{kT_\infty}$; chemical reaction parameter, $Kr = \frac{\upsilon K (C_w - C_\infty)^{p-1}}{U_w^2}$.

For the existing study, the skin friction, Nusselt as well as Sherwood number can be expressed as underneath

$$Cf = \frac{1}{2\sqrt{2}} Gr^{-3/4} Nv \left(\frac{\partial U}{\partial Y}\right)_{Y=0}; \; Nu = \frac{1}{\sqrt{2}} Gr^{-3/4} \left(\frac{\partial \theta}{\partial Y}\right)_{Y=0}; \; Sh = \frac{1}{\sqrt{2}} Gr^{-3/4} \left(\frac{\partial C}{\partial Y}\right)_{Y=0}$$

The stream function ψ along with the velocity component associated with it satisfy the continuity equation in the following way: $U = \frac{\partial \psi}{\partial Y}, V = -\frac{\partial \psi}{\partial X}$

5. Numerical computation

In the previous section of our mathematical investigation, we performed multiple computations to arrive at the dimensionless governing equations (7)–(10) and associated boundary conditions. In addition, the nonlinearity of the aforementioned equations makes it difficult and time-consuming to solve the boundary condition related time dependent partial differential equations (PDEs) analytically. Carnahan solved the differential equations by estimating derivatives with finite differences utilizing Finite Difference Methods (FDM), a class of numerical techniques utilized in numerical analysis to solve such models. The "Explicit Finite Difference Method" (EFDM) represents a numerical approach employed in the resolution of partial differential equations (PDEs), notably within the realms of computational mathematics, physics, and engineering. In instances where attaining analytical solutions proves challenging or unattainable, the EFDM method is frequently utilized to provide approximations. In the application of the Explicit Finite Difference Method, the spatial and temporal dimensions of a given PDE are discretized into a grid, and at each grid point, values are iteratively updated using explicit mathematical expressions. This method derives its name from its "explicit" nature, as it directly computes the solution at a particular time step based on the values from the preceding time step. Using finite differences, transform nonlinear partial differential equations (PDE) into a system of linear equations that can be solved by matrix algebraic techniques. This investigation employs an explicit finite difference method. Grid squares are formed within the border layer by intersecting appearances

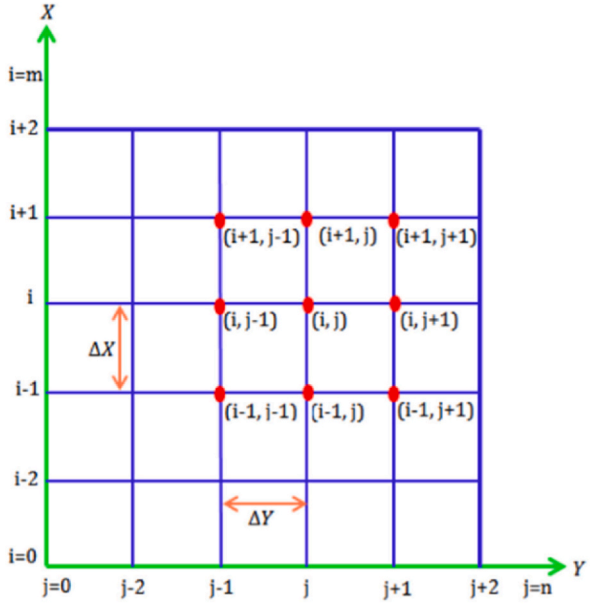

Fig. 2. Grid spacing of finite difference method [43].

that placed perpendicular to the axes X also Y (Fig. 2). Unlike the Y axis, which is determined differently, the X axis is equivalent to extending surface. During calculation, each PDE is renewed into a set of finite difference equations. The process depicted in the figure below consists of constructing a mesh or network of distinct components.

In the current work, the altitude of the plate is represented by the numerical values X (=100) and Y (=25). Additionally, the grid space is represented by m (=100) and n (=200). Hence equations (7)–(10) becomes

$$\frac{V_{i,j}-V_{i,j-1}}{\Delta Y}=\frac{U_{i-1,j}-U_{i,j}}{\Delta X} \tag{12}$$

$$U_{i,j}^{'}=U_{i,j}+Gr\theta_{i,j}\Delta\tau+GmC_{i,j}\Delta\tau-Nv\Delta\tau\frac{U_{i+1,j}-2U_{i,j}+V_{i-1,j}}{\Delta X}\left(U_{i,j}\right)^{2}-2Nv\Delta\tau U_{i,j}V_{i,j}\frac{U_{i+1,j+1}+U_{i-1,j-1}-U_{i+1,j-1}-U_{i-1,j+1}}{4\Delta X\Delta Y}$$
$$-Nv\Delta\tau\left(V_{i,j}\right)^{2}\frac{U_{i,j-1}-2U_{i,j}+U_{i,j+1}}{\left(\Delta Y\right)^{2}}-MU_{i,j}\Delta\tau+\frac{U_{i,j+1}+U_{i,j-1}-2U_{i,j}}{\left(\Delta Y\right)^{2}}\Delta\tau-\left(\frac{U_{i,j}-U_{i-1,j}}{\Delta X}\right)U_{i,j}\Delta\tau-\left(\frac{U_{i,j+1}-U_{i,j}}{\Delta Y}\right)V_{i,j}\Delta\tau \tag{13}$$

$$\theta_{i,j}^{'}=\theta_{i,j}+\Delta\tau\left[Pr^{-1}\left[1+Ra\left\{1+(\theta_{w}-1)\theta_{i,j}\right\}^{3}\right]\left(\frac{\theta_{i,j+1}-2\theta_{i,j}+\theta_{i,j-1}}{\left(\Delta Y\right)^{2}}\right)+Nt\left(\frac{\theta_{i,j+1}-\theta_{i,j}}{\Delta Y}\right)^{2}\right]$$
$$+\Delta\tau\left[Du\left(\frac{C_{i,j+1}-2C_{i,j}+C_{i,j-1}}{\left(\Delta Y\right)^{2}}\right)+Pr^{-1}\,Ra\left\{1+(\theta_{w}-1)\theta_{i,j}\right\}^{3}\left(\frac{\theta_{i,j+1}-\theta_{i,j}}{\Delta Y}\right)^{2}-U_{i,j}\left(\frac{\theta_{i,j}-\theta_{i-1,j}}{\Delta X}\right)\right] \tag{14}$$
$$+\Delta\tau\left[Ec\left(\frac{U_{i,j+1}-U_{i,j}}{\Delta Y}\right)^{2}-V_{i,j}\left(\frac{\theta_{i,j+1}-\theta_{i,j}}{\Delta Y}\right)+Nb\left(\frac{C_{i,j+1}-C_{i,j}}{\Delta Y}\,\frac{\theta_{i,j+1}-\theta_{i,j}}{\Delta Y}\right)\right]$$

$$C_{i,j}^{'}=C_{i,j}+Nt(PrNbLe)^{-1}\left(\frac{\theta_{i,j+1}-2\theta_{i,j}+\theta_{i,j-1}}{\left(\Delta Y\right)^{2}}\right)\Delta\tau+(PrLe)^{-1}\left(\frac{C_{i,j+1}-2C_{i,j}+C_{i,j-1}}{\left(\Delta Y\right)^{2}}\right)\Delta\tau-Kr\left(\gamma\theta_{i,j}+1\right)^{n}e^{\left(\frac{-AE}{\gamma\theta_{i,j}+1}\right)}C_{i,j}\Delta\tau$$
$$-U_{i,j}\left(\frac{C_{i,j}-C_{i-1,j}}{\Delta X}\right)\Delta\tau-V_{i,j}\left(\frac{C_{i,j+1}-C_{i,j}}{\Delta Y}\right)\Delta\tau \tag{15}$$

Also, the boundary conditions,

$$U_{i,0}^{n}=1,T_{i,0}^{n}=1,C_{i,0}^{n}=1$$
$$U_{i,0}^{n}=0,T_{i,L}^{n}=0,T_{i,L}^{n}=0\ \text{ where},L\rightarrow\infty$$

$i=$ mesh points along X axis; $j=$ mesh points along Y axis

$n=$ time value also, τ represents the time value and expressed as, $\tau=n\Delta\tau,n\in\mathbb{N}$.

Although the Explicit Finite Difference Method (EFDM) is a valuable numerical tool for tackling partial differential equations, it does come with certain limitations and constraints. Due to the requisite use of small time increments and fine-grained spatial

discretization to ensure stability, EFDM can become computationally demanding when addressing large-scale problems or complex systems. Additionally, EFDM is subject to stability considerations, particularly concerning the choice of time step.

6. Stability and convergence analysis

Because the EFDM was attempted to wrap up the model, a study of stability and convergence is now required to assess whether or not the model will be complete. For a particular mesh size, we could satisfy the potential stability criterion for the remaining work as follows. Additionally, the absence of excludes equation (12) from applying the stability and convergence test. Using the dimensionless *C, U* and θ procedure of stability and convergence test starts. An assumption is made by considering $e^{i\alpha X}e^{i\beta Y}$ which is the known term at time $\tau = 0$ of Fourier expansion and here $i = \sqrt{-1}$.

Now the Fourier expansion of C, *U* and θ for any time τ can be expressed as equation (16) and for $\Delta\tau$ Fourier extension for C', *U*' and θ' can be depicted as equation (17)

$$\left.\begin{array}{l} U : D(\tau)e^{i\alpha X}e^{i\beta Y} \\ \theta : E(\tau)e^{i\alpha X}e^{i\beta Y} \\ C : F(\tau)e^{i\alpha X}e^{i\beta Y} \end{array}\right\} \tag{16}$$

$$\text{Again, } \left.\begin{array}{l} U^{'} : D^{'}(\tau)e^{i\alpha X}e^{i\beta Y} \\ \theta^{'} : E^{'}(\tau)e^{i\alpha X}e^{i\beta Y} \\ C^{'} : F^{'}(\tau)e^{i\alpha X}e^{i\beta Y} \end{array}\right\} \tag{17}$$

now sequentially substituting the value of (16), (17) into (13) - (15) and considering *U*, *V* as constants the results are underneath,

$$\begin{aligned} D^{'} &= D + (1+Nv)\left((1-\cos\alpha\Delta X)U^2\frac{2\Delta\tau}{(\Delta X)^2} + (\cos\beta\Delta Y - 1)V^2\frac{2\Delta\tau}{(\Delta Y)^2}\right) + (\cos\beta\Delta Y - 1)2\Delta\tau \\ &-(1+Nv)\left(2UV\Delta\tau\frac{e^{i\alpha(X+\Delta X)}\left\{e^{i\beta(Y-\Delta Y)} - e^{i\beta(Y+\Delta Y)}\right\}}{4\Delta Y\Delta X}\right) + (GrE + GmF - M)\Delta\tau \\ &+(1+Nv)\left(2UV\Delta\tau\frac{e^{i\alpha(X-\Delta X)}\left\{e^{i\beta(Y+\Delta Y)} + e^{i\beta(Y-\Delta Y)}\right\}}{4\Delta Y\Delta X}\right) \end{aligned} \tag{18}$$

$$\begin{aligned} E^{'} &= E\left[1 + \frac{2\Delta\tau}{(\Delta Y)^2}Pr^{-1}\left[1 + Ra\{1 + (\theta_w - 1)\theta\}^3\right](\cos\beta\Delta Y - 1) + NbC\left(e^{i\beta\Delta Y} - 1\right)^2\frac{\Delta\tau}{(\Delta Y)^2}\right] \\ &+E\left[Pr^{-1}\,Ra\{1 + (\theta_w - 1)\theta\}^3\frac{\Delta\tau}{(\Delta Y)^2}\left(e^{i\beta\Delta Y} - 1\right)^2 - U\frac{\Delta\tau}{\Delta X}\left(1 - e^{i\alpha\Delta X}\right) - \frac{\Delta\tau}{\Delta Y}V\left(e^{i\beta\Delta Y} - 1\right)\right] \\ &+\left[Du\frac{2\Delta\tau}{(\Delta Y)^2}(\cos\beta\Delta Y - 1)\right]F + D\left[Ec\frac{\Delta\tau}{(\Delta Y)^2}U\left(e^{i\beta\Delta Y} - 1\right)^2\right] \end{aligned} \tag{19}$$

$$\begin{aligned} F^{'} &= E\left[(\cos\beta\Delta Y - 1)Nt(Nb\,Pr\,Le)^{-1}\frac{2\Delta\tau}{(\Delta Y)^2}\right] - F\left[U\frac{\Delta\tau}{\Delta X}\left(1 - e^{-i\alpha\Delta X}\right) + V\frac{\Delta\tau}{\Delta Y}\left(e^{i\beta\Delta Y} - 1\right)\right] \\ &+F\left[1 + \frac{2\Delta\tau}{(\Delta Y)^2}(Pr\,Le)^{-1}(\cos\beta\Delta Y - 1) - \Delta\tau Kr(1+\gamma\theta)^n e^{\left(\frac{-AE}{1+\gamma\theta}\right)}\right] \end{aligned} \tag{20}$$

Subsequently, we can rewrite equations (18)–(20) as,

$$\left.\begin{array}{l} D^{'} = A_1D + A_2E + A_3F \\ E^{'} = A_4D + A_5E + A_6F \\ F^{'} = A_7E + A_8F \end{array}\right\} \tag{21}$$

where,

$$\begin{aligned} A_1 &= 1 + Nv\left[(1-\cos\alpha\Delta X)U^2\frac{2\Delta\tau}{(\Delta X)^2} + (\cos\beta\Delta Y - 1)V^2\frac{2\Delta\tau}{(\Delta Y)^2}\right] - V\frac{\left(e^{i\beta\Delta Y} - 1\right)}{\Delta Y}\Delta\tau - Nv\left[2UV\Delta\tau\frac{e^{i\alpha(X+\Delta X)}\left\{e^{i\beta(Y-\Delta Y)} - e^{i\beta(Y+\Delta Y)}\right\}}{4\Delta Y\Delta X}\right] \\ &-U\frac{(1 - e^{-i\alpha\Delta X})}{\Delta X}\Delta\tau \\ &+Nv\left[2UV\Delta\tau\frac{e^{i\alpha(X-\Delta X)}\left\{e^{i\beta(Y-\Delta Y)} - e^{i\beta(Y+\Delta Y)}\right\}}{4\Delta Y\Delta X}\right] - M\Delta\tau + \frac{2\Delta\tau(\cos\beta\Delta Y - 1)}{(\Delta Y)^2} \end{aligned}$$

$$A_2 = Gr; \quad A_3 = Gm; \quad A_4 = Ec\frac{\Delta\tau}{(\Delta Y)^2}U\left(e^{i\beta\Delta Y}-1\right)^2$$

$$A_5 = 1+\frac{2\Delta\tau}{(\Delta Y)^2}(\cos\beta\Delta Y-1)Pr^{-1}\left(1+Ra\{1+(\theta_w-1)\theta\}^3\right)-U\frac{\Delta\tau}{\Delta X}\left(1-e^{i\alpha\Delta X}\right)-V\frac{\Delta\tau}{\Delta Y}\left(e^{i\beta\Delta Y}-1\right)$$

$$+\frac{Ra}{Pr}\{1+(\theta_w-1)\theta\}^3\frac{\Delta\tau}{(\Delta Y)^2}\left(e^{i\beta\Delta Y}-1\right)^2+\frac{\Delta\tau}{(\Delta Y)^2}NbC\left(e^{i\beta\Delta Y}-1\right)^2+Nt\theta\left(e^{i\beta\Delta Y}-1\right)^2\frac{\Delta\tau}{(\Delta Y)^2}$$

$$A_6 = Du\frac{2\Delta\tau}{(\Delta Y)^2}(\cos\beta\Delta Y-1); \quad A_7 = Nt(Pr\,NbLe)^{-1}\frac{2\Delta\tau}{(\Delta Y)^2}(\cos\beta\Delta Y-1)$$

$$A_8 = 1+\frac{2\Delta\tau}{(\Delta Y)^2}(Pr\,Le)^{-1}(\cos\beta\Delta Y-1)-\Delta\tau Kr(1+\gamma\theta)^n e^{\left(\frac{-\Delta E}{1+\gamma\theta}\right)}-\frac{\Delta\tau}{\Delta X}U\left(1-e^{-i\alpha\Delta X}\right)-\frac{\Delta\tau}{\Delta Y}V\left(e^{i\beta\Delta Y}-1\right)$$

now representing equation (21)

$$\begin{bmatrix}D'\\E'\\F'\end{bmatrix}=\begin{bmatrix}A_1 & A_2 & A_3\\A_4 & A_5 & A_6\\0 & A_7 & A_8\end{bmatrix}\begin{bmatrix}D\\E\\F\end{bmatrix};\therefore\eta'=T'\eta$$

where,

$$\eta'=\begin{bmatrix}D'\\E'\\F'\end{bmatrix},T'=\begin{bmatrix}A_1 & A_2 & A_3\\A_4 & A_5 & A_6\\0 & A_7 & A_8\end{bmatrix}\text{ and }\eta=\begin{bmatrix}D\\E\\F\end{bmatrix}$$

It is challenging enough for various research value of T'.Consequently, not a large step $\Delta\tau\to0$ is being taken to determine the matrix's eigenvalues. Besides, we end up here with considering $A_2\to0, A_3\to0, A_4\to0, A_6\to0, A_7\to0$, consequently the matrix T' re-casted as

$$T'=\begin{bmatrix}A_1 & 0 & 0\\0 & A_5 & 0\\0 & 0 & A_8\end{bmatrix}$$

So considering the values of T' as $A_1=\lambda_1, A_5=\lambda_2, A_8=\lambda_3$, these eigenvalues could not surpass unity in modulus that is

$$|A_1|\le 1, |A_2|\le 1, |A_3|\le 1 \tag{22}$$

$$\text{Choosing } a=\Delta\tau, b=U\frac{\Delta\tau}{\Delta X}, c=|-V|\frac{\Delta\tau}{\Delta Y}, d=\frac{2\Delta\tau}{(\Delta Y)^2}, e=\frac{2\Delta\tau}{(\Delta X)^2}, f=\frac{2\Delta\tau}{\Delta X\Delta Y}\text{ are obtained} \tag{23}$$

Here, the numbers a, b, c, d, e, and f are real and positive. Considering V and U are respectively positive and negative. For A_1, A_5, A_8, $\beta\Delta Y=n\pi$ and $\alpha\Delta X=m\pi$ the greatest modulus appears where $n, m\neq$ even integers. Using the conditions mentioned in equations (22) and (23), the following equations may be obtained as,

$$A_1 = 1-2\left[d-\frac{Nv}{2}\left\{U^2e+V^2d+\frac{fUV}{4}\right\}+\frac{Ma}{2}+b+c\right]$$

$$A_5 = 1-2\left[b+c-dNt\theta-dNbC+\frac{d}{\mathrm{Pr}}\left\{1+2Ra\{1+(\theta_w-1)\theta\}^3\right\}\right]$$

$$A_8 = 1-2\left[b+c+\frac{d}{Pr\,Le}+\frac{a}{2}Kr(1+\gamma\theta)^n e^{\left(\frac{-\Delta E}{1+\gamma\theta}\right)}\right]$$

here, -1 is the maximum bound negative value of A_1, A_5, A_8. As a result, the following are the stability postulates

$$\frac{2\Delta\tau}{(\Delta Y)^2}+U\frac{\Delta\tau}{\Delta X}-\frac{Nv}{2}\left\{\frac{UV}{4}\frac{2\Delta\tau}{\Delta X\Delta Y}+V^2\frac{2\Delta\tau}{(\Delta Y)^2}+U^2\frac{2\Delta\tau}{(\Delta X)^2}\right\}+\frac{M\Delta\tau}{2}+V\frac{\Delta\tau}{\Delta Y}\le 1$$

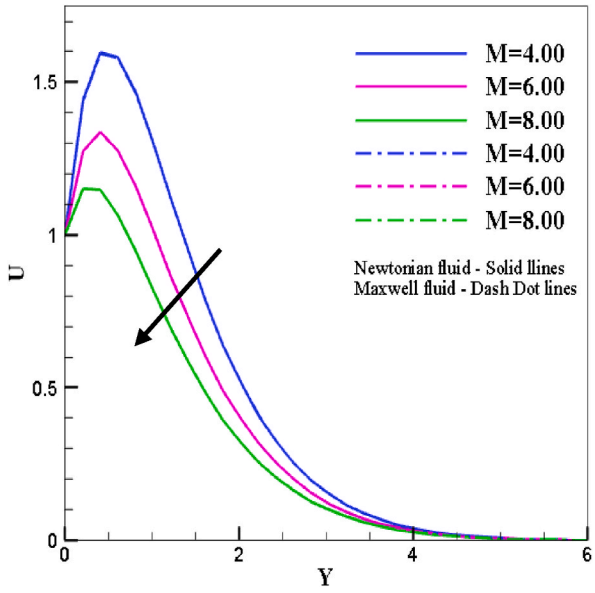

Fig. 3. Influence of magnetic parameter M on velocity U.

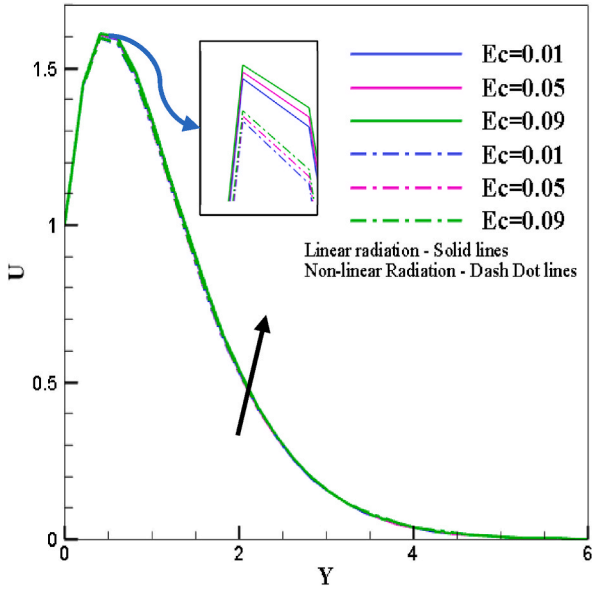

Fig. 4. Influence of Eckert number (Ec) on velocity profile U.

$$U\frac{\Delta\tau}{\Delta X} - Nb\frac{2\Delta\tau}{(\Delta Y)^2}C + V\frac{\Delta\tau}{\Delta Y} + \frac{2\Delta\tau}{(\Delta Y)^2}Pr^{-1}\left\{1 + 2Ra\{1 + (\theta_w - 1)\theta\}^3\right\} - Nt\frac{2\Delta\tau}{(\Delta Y)^2}\theta \leq 1$$

$$U\frac{\Delta\tau}{\Delta X} + V\frac{\Delta\tau}{\Delta Y} + \frac{2\Delta\tau}{(\Delta Y)^2}(Pr\,Le)^{-1} + \frac{\Delta\tau}{2}Kr(1+\gamma\theta)^n e^{\left(\frac{-AE}{1+\gamma\theta}\right)} \leq 1$$

here, with initial values of fundamental phenomena with $\Delta X = 0.20$, $\Delta\tau = 0.0005$, $\Delta Y = 0.25$ The present work's convergence criterion would be the following $Le \geq 0.016$ and $Pr \geq 0.08$.

7. Results and discussion

This section examines a concise report of a physical event. Earlier in this project, for the mathematical analysis, we employed the

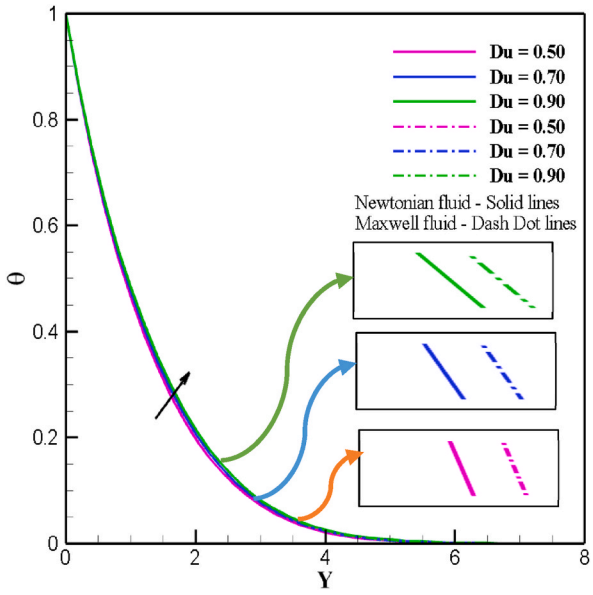

Fig. 5. Impact of *Du* (Dufour number) on Temperature outline.

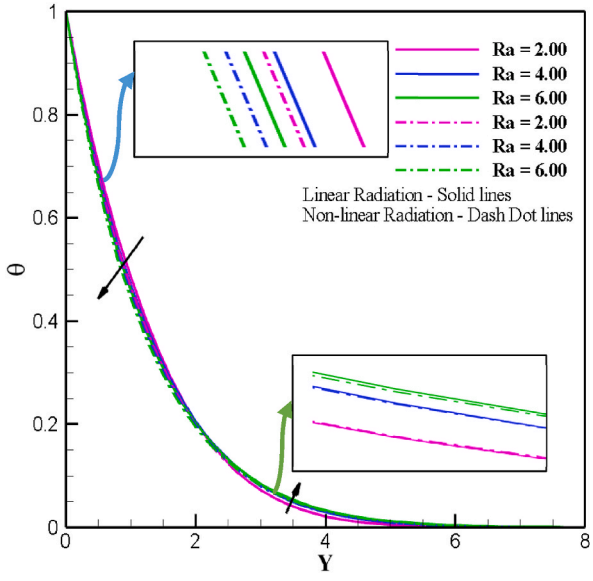

Fig. 6. Stimulus of thermal radiation (*Ra*) on the temperature outline.

explicit finite difference method; presently, we employ Visual FORTRAN software for the numerical analysis. In addition, the stimulus of various considerations on the profiles of concentration, temperature, and dimensionless velocity is explored in this ongoing study. The effect of the parameters Cf, *Sh* and *Nu*, i.e., skin friction, Sherwood, Nusselt number, is visually evaluated as a response. In addition, the contour isothermal line and streamline are graphically represented. The competent parameters are $M = 4, 6, 8$, $\mathrm{Pr} = 0.71, 1.00, 1.38$, $Ra = 2, 4, 6$, $AE = 1, 4\ 7$, $Ec = 0.01, 0.05, 0.09$, $Du = 0.50, 0.70, 0.90$, $Nt = 0.50, 1.50, 2.50$, and $Nb = 0.30, 1.30, 2.50$.

The effect of the magnetic parameter *M* upon dimensionless velocity profile for fluids that are Newtonian and Maxwell are represented graphically in Fig. 3. The figure exhibits the development of the Maxwell fluid's velocity profiles. Newtonian fluid, however, exhibits the same phenomena. The velocity profile grows throughout the initial phase of the magnetic parameter, as seen in the illustration. This implies that in the presence of a magnetic parameter, the boundary layer velocity profile, which reduces as the induced Lorentz force increases, increases. As a consequence, an increase in Lorentz force will restrict the fluid path and reduction the fluid velocity. This observation is supported by the published paper of Reza-E-Rabbit et al. [25], in which the authors illustrated the impressions of magnetic constraint on a non-Newtonian fluid. Variations in the magnetic constraint, conversely, have no discernible

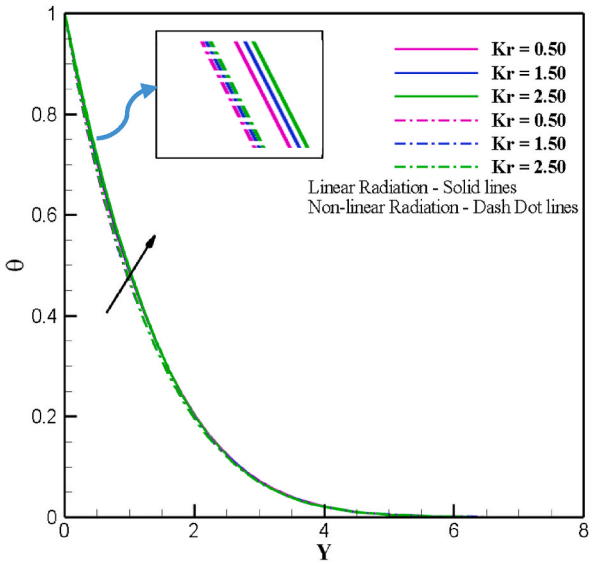

Fig. 7. Impacts of chemical reaction (*Kr*) on temperature profile.

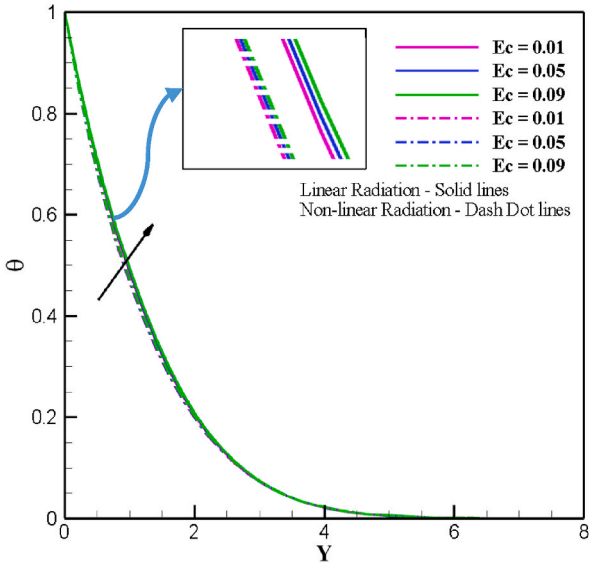

Fig. 8. Impression of Eckert number (*Ec*) on temperature profile.

effect on the wideness of the hydrodynamic boundary layer.

Fig. 4 illustrates the impact of *Ec* upon the velocity profile, which influences linear radiation more than nonlinear radiation. According to physical behavior, increasing *Ec* generates a progressive increase throughout velocity distribution. The Eckert number is the relationship involving the kinetic energy and the boundary layer's temperature difference of the flows, and it is often used to characterize heat transfer inefficiency. In accordance with the in recent times issued article of Kumar et al. [56], authors made similar observations as this ongoing study and obtained similar results.

Next Fig. 5 demonstrates the implication of the Dufour number upon the temperature profile. Temperature profile grows as the Dufour number increases in this graph. Due to the presence of Dufour number energy, which generates heat flux, the temperature profile is increased. This is happening for both fluids, with the Maxwell fluid's Dufour number developing a little bit more than the Newtonian fluid's. The published work of Biswal et al. [57] validates an analogous phenomenon observed in Casson fluid.

Fig. 6 illustrates the manner in which the thermal radiation parameter affects the temperature profile, showing how it gradually drops as the thermal radiation value rises. This pattern holds true for both linear and nonlinear radiation. Greater *Ra* values predominate in conductivity. As a consequence of enhanced radiation, the temperature rises. Moreover, *Ra* accelerates the variation in heat flux. The resulting finding is validated by earlier Miroshnichenko et al. [58] comparable occurrences for *Ra* over concentration

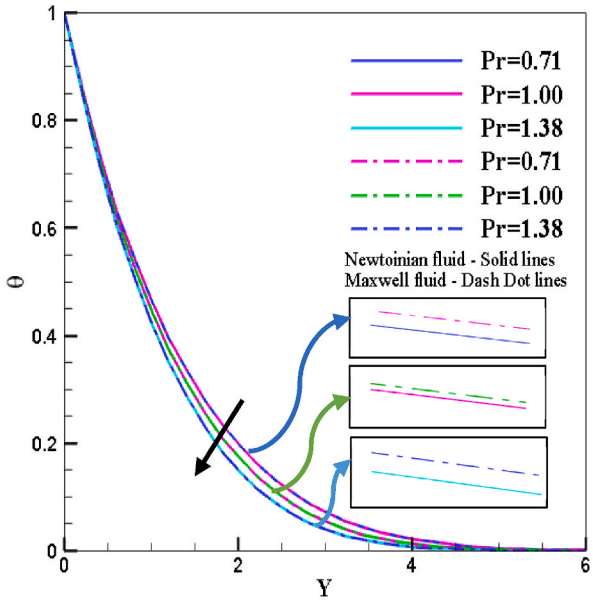

Fig. 9. Impact of Prandtl number (*Pr*) on the Temperature Outline θ.

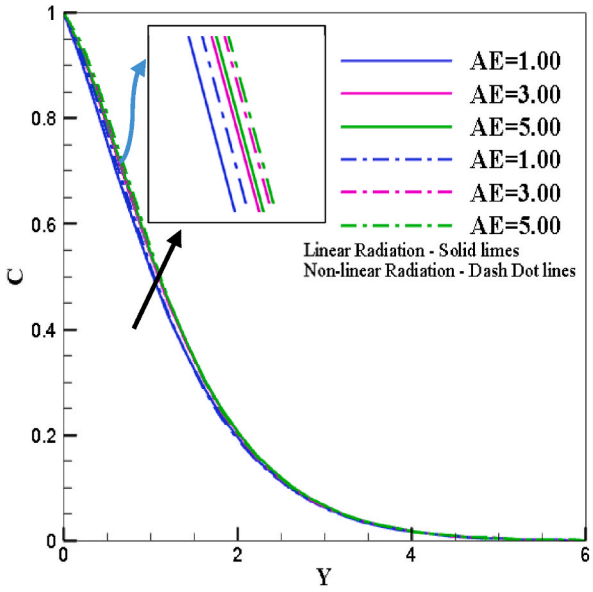

Fig. 10. Impression of Activation Energy on Concentration Profile with linear and nonlinear radiation.

lines.

Fig. 7 investigates the consequence of chemical reaction parameter upon temperature profile and illustrates a reverse phenomenon for nonlinear radiation, as the chemical reaction constraint rises, the temperature profile for both radiations steadily rises. This increases the likelihood of fluid particle collisions, which increases the likelihood of a temperature rise due to an increase in *Kr*. As exemplified in Fig. 8, as the Eckert number (*Ec*) rises, so does the temperature profile for both radiation. The fluid's coefficient of expansion (*Ec*) rises as a result of frictional heating. The Eckert number is the result of the product of the kinetic energy and the specific enthalpy difference between the fluid and the wall. Consequently Eckert number rises, work is conducted against the viscous fluid stresses, work is carried out against the strains of the viscous fluid, and kinetic energy is transformed into internal energy. As a consequence, a growth in *Ec* causes an upturn in the temperature outline.

Fig. 9 depicts the implication of Prandtl numbers upon the temperature profile for Maxwell and Newtonian flow. From the definition of Prandtl number, it is evident that liquids with a high Pr will have a low thermal diffusivity, as shown in the figure. Except for Maxwell fluid, which has a swiftly decreasing density, the difference between two fluids is negligible. This Maxwell fluid phenomenon

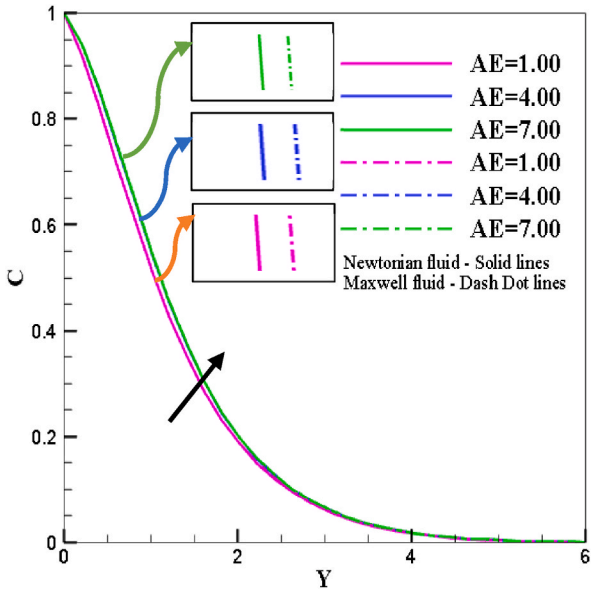

Fig. 11. Influence of Activation Energy (*AE*) on Concentration Profile for both fluid.

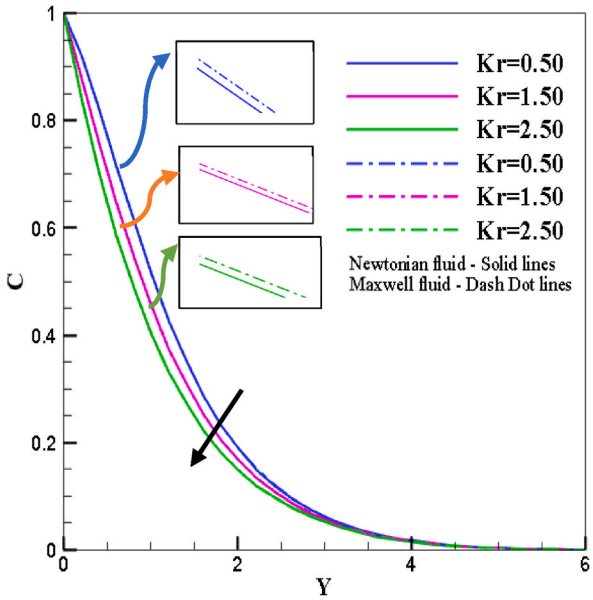

Fig. 12. Stimulus of *Kr* (Chemical reaction) on Concentration Outline for both fluids.

is remarkable for the development of cancer treatment, a novel field of study. This is also supported by a study by Deepthi et al. [59], in which a related occurrence was noted. Fig. 10 observes the impacts of AE on linear and nonlinear radiation concentration profiles. The presence of AE explains why nonlinear radiation is relatively more concentrically distributed. The temperature control mechanism must be as strong to withstand this as the energy requires of starting a chemical reaction using the available reactants. Consequently, the activation energy of nonlinear radiation has already been calculated utilizing the concentration profile. The second observation was made when the activation energy grew exponentially and mass transmission began. This phenomenon is utilized extensively in nuclear reactions, industrial processes, and medical reasoning.

Activation Energy's impact on the concentration profile of Maxwell and Newtonian fluids are illustrated in Fig. 11 by the increase in the concentric profile caused by the activation energy parameter *AE*. The Arrhenius activation energy equation's final term states that a boost in activation energy induces a decrease in activation energy; as a consequence, the concentration profile for both fluids rises. Sabir et al. [60] previously studied the impacts of AE and discovered a comparable effect on the concentration profile for non-Newtonian fluid. Figs. 12 and 13 depict the chemical reaction parameter *Kr*, which demonstrates a slight inhibition of the

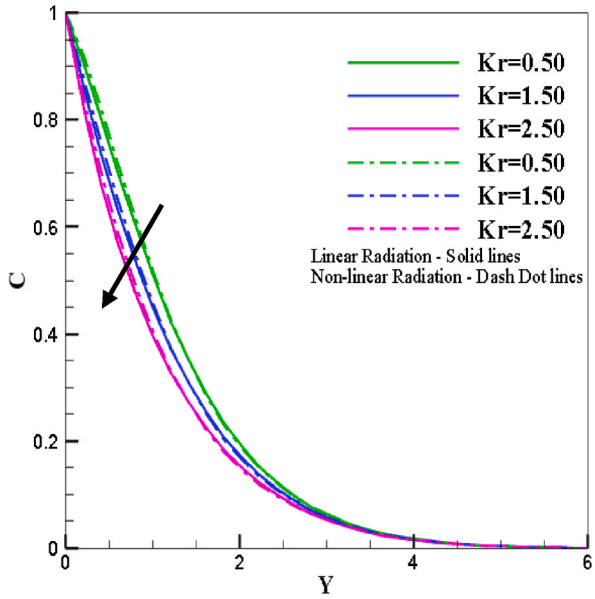

Fig. 13. Impact of (*Kr*) on the Concentration Profile with linear and nonlinear radiation.

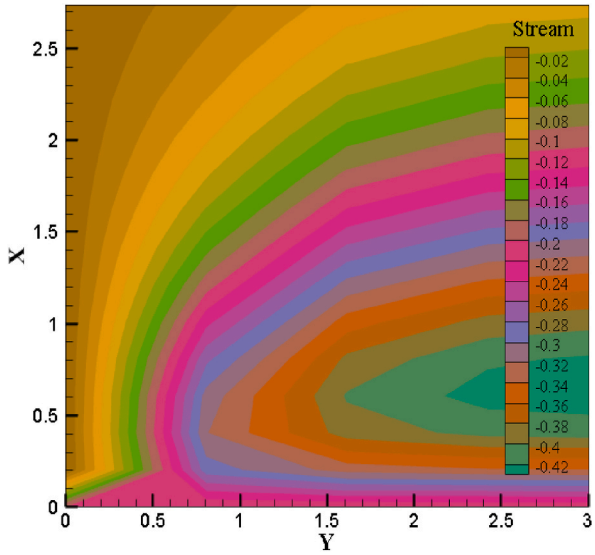

Fig. 14. Advanced visualization of Streamlines for various *Nt*.

chemical reaction along the concentration curve. Clearly, the concentration profiles of both fluids, as well as linear and nonlinear radiation, decrease as the chemical reaction parameter increases. Non-linear radiation is, however, considerably superior to linear radiation.

Figs. 14–17 depicts the contour design-generated streamline in both flood view and line view. As the moving particle is ultimately considered, the streamline is frequently derived from the motion of massless fluid particles whose velocity is tangent to every path point. Physically, an isotherm is depicted on a graph by a curve connecting points of equal temperature. Figs. 15 and 17 depict the impact of p-radiation on isothermal lines. A particular observation from Fig. 17 reveals that rapid energy development of fluid causes molecules to heat up for strong thermophoresis parameters ($Nt = 0.50, 1.5, 2.50$), leading to an increase in the wideness of the thermal boundary layer and a comparison line for both linear and nonlinear radiation. Figs. 18–21 similarly depicts the flood view as well as line view of streamlines and the isothermal line in the presence of the Brownian motion constraint (*Nb*). Increasing the Brownian parameter raises the isothermal line.

Figs. 22–24 provide a thoughtful study of the fluctuation in skin friction (Cf), Nusselt number (*Nu*), and Sherwood number (*Sh*) in response to variations in the radiation parameter (*Ra*). The information clarifies how radiation affects both Maxwell fluid systems and

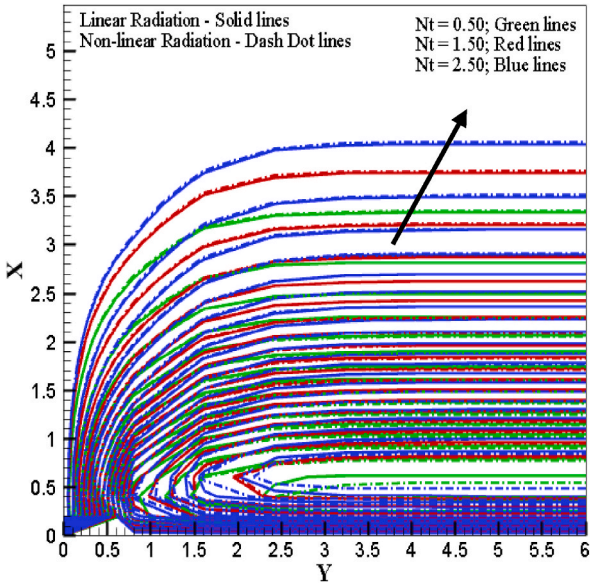

Fig. 15. Streamlines as Line view for various *Nt*.

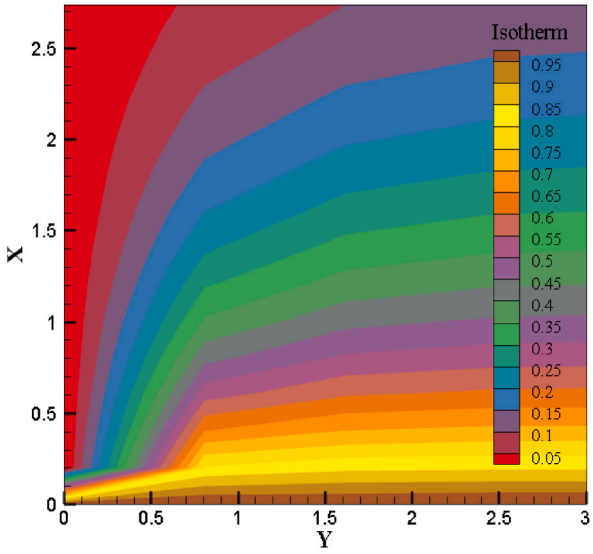

Fig. 16. Advanced visualization of Isothermal Line for Various *Nt*.

non-Newtonian fluid systems, highlighting the unique impacts of radiation.

Skin friction (Cf), an important fluid dynamics parameter, responds significantly to fluctuations brought on by radiation. The fundamental physical phenomena is that heat transmission at the fluid-solid interface is accelerated by thermal radiation, especially nonlinear radiation. The fluid's surface friction is significantly altered when the radiation parameter (Ra) rises, which is visible as a shift in Fig. 22. This phenomena has significant ramifications for several technical applications, including aerospace, where reducing skin friction is critical for lowering drag and improving overall performance. With implications for reducing drag and aerospace applications, the results show that thermal radiation, in particular nonlinear radiation, has a significant influence on skin friction. The Nusselt number (*Nu*), which can be seen in Fig. 23, responds to changes in the radiation parameter somewhat more subtly. This mismatch is explained by the fact that the Nusselt number mainly describes convective heat transfer, which is less strongly influenced by radiation than skin friction. When radiation only plays a minor part in heat transport, such in the cooling systems of electronic devices, *Nu*, which measures the temperature differential across a boundary layer, is frequently more pertinent. The results show that the Nusselt number is less sensitive and has a less significant impact on heat transfer processes, even if radiation still has an impact. In a variety of industrial applications where precise control of heat and mass transport is crucial, these discoveries have real-world applications.

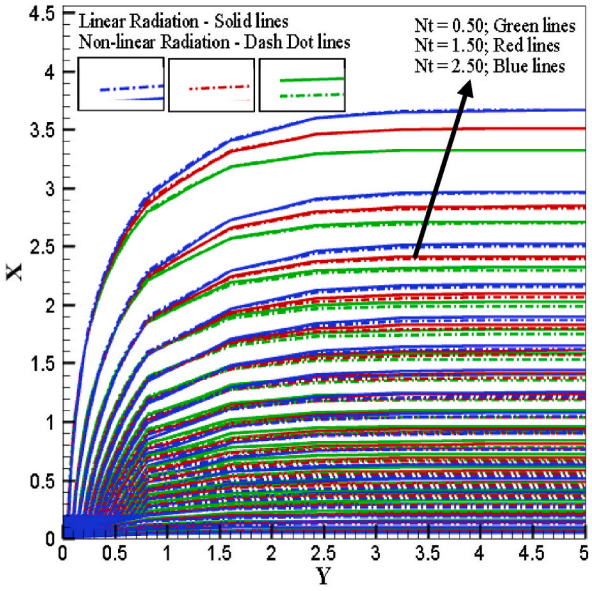

Fig. 17. Isothermal line view for various *Nt*.

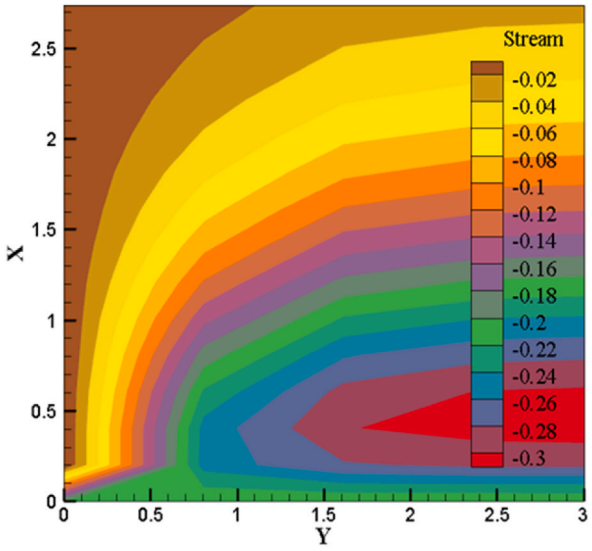

Fig. 18. Streamlines with Advanced visualization for various *Nb*.

The mass transfer-related Sherwood number (*Sh*) turns out to be the most responsive to changes in the radiation parameter (*Ra*). This increased sensitivity results from the strong relationship between temperature fluctuations in the medium and mass transfer mechanisms. The physical explanation is that heat radiation affects the concentration gradients, which in turn affects the mass transfer rates. The Sherwood number, which is more impacted by radiation impacts and is shown in Fig. 24, is particularly relevant in situations where it is crucial to regulate the spread of species. For example, in trash incineration procedures, radiation-induced temperature increases lead to larger Sherwood numbers, which imply improved mass transfer rates. This is necessary for effective waste management and combustion. The results show that the Sherwood number is strongly influenced by radiation, which makes it important in situations like waste combustion where improved mass transfer is necessary.

8. Validation of the outcomes

Fig. 25 depicts a validity check using the published work of Ali et al. [34] and Reza-e-Rabbi et al. [43]. The results have been validated in the Nusselt number region as well as taking *Ra* at values 1,2, and 3 via a bar illustration. It indicates that the most recent outcomes are very in line with prior ones.

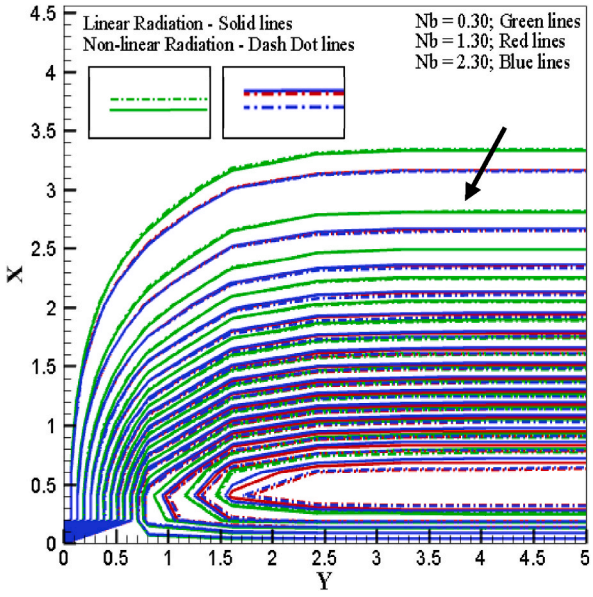

Fig. 19. Line view for various *Nb*.

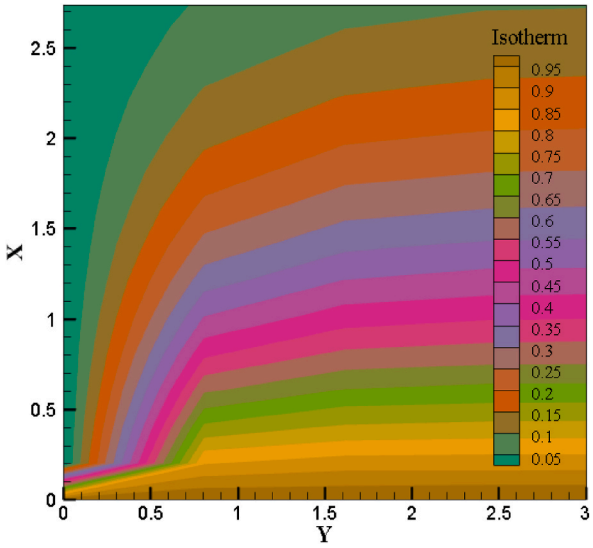

Fig. 20. Isothermal line (flood view) for various *Nb*.

9. Conclusions

The aim of this inquiry is to scrutinize the influence of activation energy in conjunction with nonlinear radiation on the flow characteristics of a Magnetohydrodynamic (MHD) Maxwell fluid and a nanoscale non-Newtonian liquid diffusing over a stretched sheet. Several relevant dimensionless parameters are harnessed to facilitate this pursuit. Numerical computations are carried out employing the explicit finite difference (EFD) technique. Additionally, we undertake a stability analysis and convergence tests to ascertain the robustness and reliability of the solution. Subsequently, a series of experiments is scheduled to investigate the impact of various parameters on the concentration, velocity, and temperature profiles. As a result, we present isothermal and streamlined profiles. The accumulation of multiple observations enables us to draw the following conclusions:

➢ In the presence of a magnetic field, the Lorentz force becomes more pronounced, yet it imparts a more pronounced reduction in fluid flow velocity, especially when applied to non-Newtonian fluids, which display heightened susceptibility to this phenomenon.

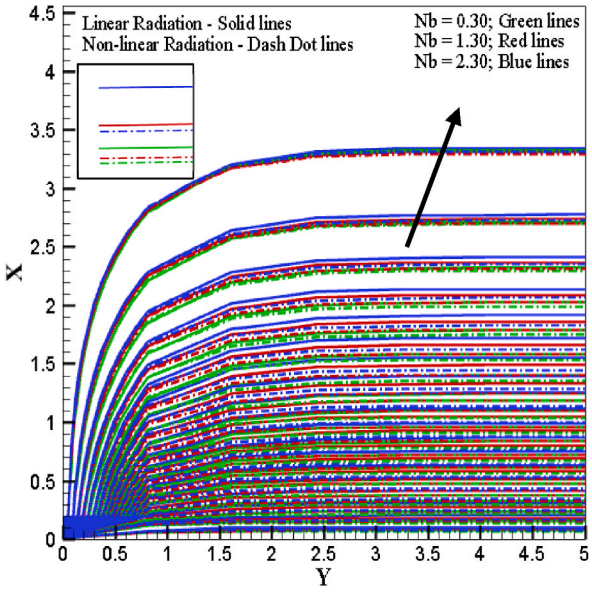

Fig. 21. Line view for various *Nb*.

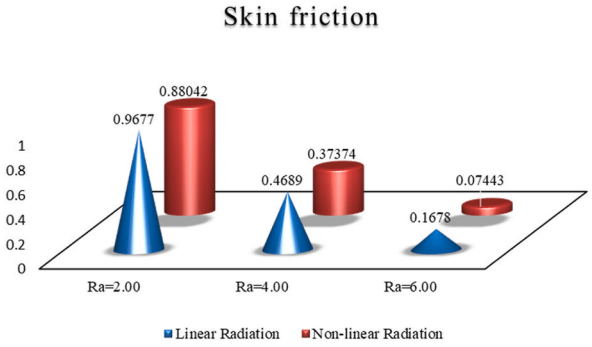

Fig. 22. Variation in the skin friction caused by *Ra*.

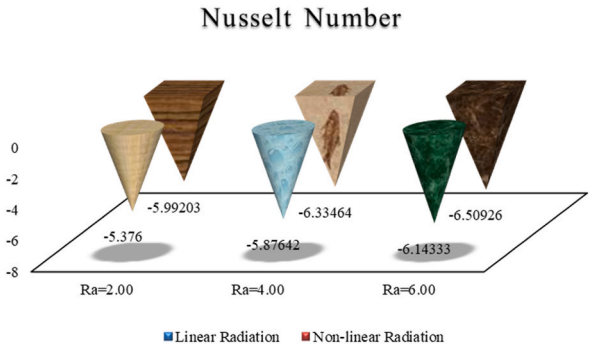

Fig. 23. Variation in the Nusselt number caused by *Ra*.

- ➢ The Dufour number, a chemical reaction-related parameter, amplifies the temperature profile in Maxwell fluids compared to Newtonian fluids, showing a clear bias toward linear radiation effects rather than nonlinear ones in the temperature profile.
- ➢ Kr decelerates concentration field changes while promoting nonlinear radiation effects in the temperature profile, whereas the Arrhenius activation energy for nonlinear radiation and Maxwell fluids exhibits an overall increase in both profiles.

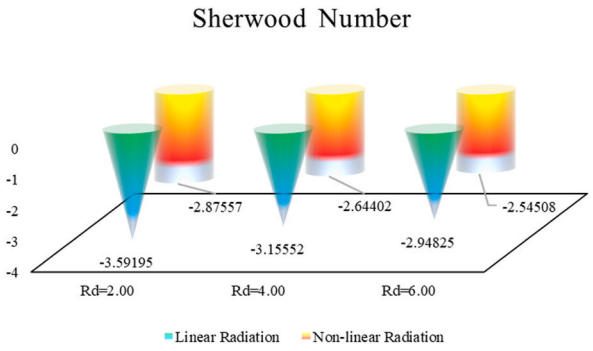

Fig. 24. Variation of Sherwood number caused by *Ra*.

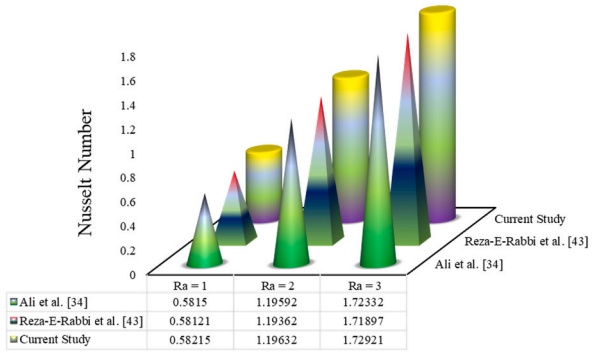

Fig. 25. Validation by comparing with previous study.

- ➢ The Nusselt number reveals sensitivity to linear radiation, whereas the skin friction coefficient and Sherwood number profiles exhibit a responsive behavior to nonlinear radiation in the presence of *M*, *Du*, *Kr*, and *Ra*.
- ➢ The combined influence of thermophoresis and Brownian motion parameters enhances both streamlines and isothermal lines, culminating in an improved response to nonlinear radiation.

The prospective uses of this theoretical examination extend to a broad spectrum of non-Newtonian fluids, encompassing diverse types such as Casson, Bingham, micropolar, and third- or fourth-grade fluids. These applications stand to gain by integrating the intricacies of exothermic/endothermic reactions, the involvement of microorganisms, quadratic convection, exponential heat generation, and assorted other phenomena. Furthermore, the forthcoming prospects entail exploring this analysis through an array of advanced methodologies, including the utilization of exponential stretching sheets, inclined stretching sheets, double stretching sheets, and cylindrical surfaces. It is noteworthy that empirical calculations always possess the potential to challenge and invalidate any theoretical conjecture.

Data availability

The data that has been used is confidential.

CRediT authorship contribution statement

Fariha Ahmed: Writing - original draft, Methodology, Investigation, Conceptualization. **Sk Reza-E-Rabbi:** Writing - review & editing, Supervision, Methodology, Investigation, Conceptualization. **Md Yousuf Ali:** Writing - review & editing, Validation, Methodology, Investigation, Data curation. **Lasker Ershad Ali:** Methodology, Investigation. **Ariful Islam:** Validation, Conceptualization. **Md Azizur Rahman:** Validation, Methodology. **Raju Roy:** Investigation, Data curation. **Md Rafiqul Islam:** Investigation. **Sarder Firoz Ahmmed:** Writing - review & editing, Methodology, Investigation, Conceptualization.

Declaration of competing interest

The authors declare that they have no known competing financial interests or personal relationships that could have appeared to influence the work reported in this paper.

References

[1] C.M. Ionescu, I.R. Birs, D. Copot, C.I. Muresan, R. Caponetto, Mathematical modelling with experimental validation of viscoelastic properties in non-Newtonian fluids, Philosophical Transactions of the Royal Society A 378 (2172) (2020) 20190284, https://doi.org/10.1098/rsta.2019.0284.

[2] T.H. Zhao, M.I. Khan, Y.M. Chu, Artificial neural networking (ANN) analysis for heat and entropy generation in flow of non-Newtonian fluid between two rotating disks, Mathematical Methods in the Applied Sciences (2021), https://doi.org/10.1002/mma.7310.

[3] W.L. Zhu, A. Beauchamp, Generic three-dimensional model of freeform surface polishing with non-Newtonian fluids, Int. J. Mach. Tool Manufact. 172 (2022) 103837, https://doi.org/10.1016/j.ijmachtools.2021.103837.

[4] G. Finotello, S. De, J.C. Vrouwenvelder, J.T. Padding, K.A. Buist, A. Jongsma, J.A.M. Kuipers, Experimental investigation of non-Newtonian droplet collisions: the role of extensional viscosity, Exp. Fluid 59 (7) (2018) 1–16, https://doi.org/10.1007/s00348-018-2568-2.

[5] A.H. Pordanjani, S. Aghakhani, M. Afrand, M. Sharifpur, J.P. Meyer, H. Xu, G. Cheraghian, Nanofluids: physical phenomena, applications in thermal systems and the environment effects-a critical review, J. Clean. Prod. 320 (2021) 128573, https://doi.org/10.1016/j.jclepro.2021.128573.

[6] M. Ramezanizadeh, M.A. Nazari, M.H. Ahmadi, E. Açıkkalp, Application of nanofluids in thermosyphons: a review, J. Mol. Liq. 272 (2018) 395–402, https://doi.org/10.1016/j.molliq.2018.09.101.

[7] M.H. Ahmadi, A. Mirlohi, M.A. Nazari, R. Ghasempour, A review of thermal conductivity of various nanofluids, J. Mol. Liq. 265 (2018) 181–188, https://doi.org/10.1016/j.molliq.2018.05.124.

[8] P. Puri, Rotating flow of an elastico-viscous fluid on an oscillating palte, ZAMM-Journal of Applied Mathematics and Mechanics/Zeitschrift für Angewandte Mathematik und Mechanik 54 (10) (1974) 743–745, https://doi.org/10.1002/zamm.19740541015.

[9] C. Fetecau, S.C. Prasad, K.R. Rajagopal, A note on the flow induced by a constantly accelerating plate in an Oldroyd-B fluid, Appl. Math. Model. 31 (4) (2007) 647–654, https://doi.org/10.1016/j.apm.2005.11.032.

[10] M.N. Khan, S. Nadeem, S. Ahmad, A. Saleem, Mathematical analysis of heat and mass transfer in a Maxwell fluid, Proc. IME C J. Mech. Eng. Sci. 235 (20) (2021) 4967–4976, https://doi.org/10.1177/0954406220976704.

[11] U. Farooq, D. Lu, S. Munir, M. Ramzan, M. Suleman, S. Hussain, MHD flow of Maxwell fluid with nanomaterials due to an exponentially stretching surface, Sci. Rep. 9 (1) (2019) 1–11, https://doi.org/10.1038/s41598-019-43549-0.

[12] C. Fetecau, R. Ellahi, S.M. Sait, Mathematical analysis of Maxwell fluid flow through a porous plate channel induced by a constantly accelerating or oscillating wall, Mathematics 9 (1) (2021) 90, https://doi.org/10.3390/math9010090.

[13] T. Hayat, S. Ahmad, M.I. Khan, A. Alsaedi, Simulation of ferromagnetic nanomaterial flow of Maxwell fluid, Results Phys. 8 (2018) 34–40, https://doi.org/10.1016/j.rinp.2017.11.021.

[14] K. Hosseinzadeh, M. Gholinia, B. Jafari, A. Ghanbarpour, H. Olfian, D.D. Ganji, Nonlinear thermal radiation and chemical reaction effects on Maxwell fluid flow with convectively heated plate in a porous medium, Heat Tran. Asian Res. 48 (2) (2019) 744–759, https://doi.org/10.1002/htj.21404.

[15] S.A. Shehzad, F. Mabood, A. Rauf, I. Tlili, Forced convective Maxwell fluid flow through rotating disk under the thermophoretic particles motion, Int. Commun. Heat Mass Tran. 116 (2020) 104693, https://doi.org/10.1016/j.icheatmasstransfer.2020.104693.

[16] S. Reza-E-Rabbi, S.M. Arifuzzaman, T. Sarkar, M.S. Khan, S.F. Ahmmed, Explicit finite difference analysis of an unsteady MHD flow of a chemically reacting Casson fluid past a stretching sheet with Brownian motion and thermophoresis effects, J. King Saud Univ. Sci. 32 (1) (2020) 690–701, https://doi.org/10.1016/j.jksus.2018.10.017.

[17] H. Alfvén, Existence of electromagnetic-hydrodynamic waves, Nature 150 (3805) (1942) 405–406, https://doi.org/10.1038/150405d0.

[18] Z. Hussain, R. Zeesahan, M. Shahzad, M. Ali, F. Sultan, A.M. Anter, N. Khan, An optimised stability model for the magnetohydrodynamic fluid, Pramana 95 (1) (2021) 1–7, https://doi.org/10.1007/s12043-020-02043-3.

[19] X. Chen, W. Yang, X. Zhang, F. Liu, Unsteady boundary layer flow of viscoelastic MHD fluid with a double fractional Maxwell model, Appl. Math. Lett. 95 (2019) 143–149, https://doi.org/10.1016/j.aml.2019.03.036.

[20] S.A. Khan, T. Hayat, M.I. Khan, A. Alsaedi, Salient features of Dufour and Soret effect in radiative MHD flow of viscous fluid by a rotating cone with entropy generation, Int. J. Hydrogen Energy 45 (28) (2020) 14552–14564, https://doi.org/10.1016/j.ijhydene.2020.03.123.

[21] K. Jabeen, M. Mushtaq, R.M. Akram Muntazir, Analysis of MHD fluids around a linearly stretching sheet in porous media with thermophoresis, radiation, and chemical reaction, Math. Probl Eng. (2020), https://doi.org/10.1155/2020/9685482, 2020.

[22] N.F.M. Noor, Analysis for MHD flow of a Maxwell fluid past a vertical stretching sheet in the presence of thermophoresis and chemical reaction, World Acad. Sci., Eng. Technol 64 (2012) 1019–1023, https://doi.org/10.5281/zenodo.1332468.

[23] A.T. Akinshilo, Mixed convective heat transfer analysis of MHD fluid flowing through an electrically conducting and non-conducting walls of a vertical micro-channel considering radiation effect, Appl. Therm. Eng. 156 (2019) 506–513, https://doi.org/10.1016/j.applthermaleng.2019.04.100.

[24] I. Chabani, F. Mebarek-Oudina, A.A.I. Ismail, MHD flow of a hybrid nano-fluid in a triangular enclosure with zigzags and an elliptic obstacle, Micromachines 13 (2) (2022) 224, https://doi.org/10.3390/mi13020224.

[25] S. Reza-E-Rabbi, S.F. Ahmmed, S.M. Arifuzzaman, T. Sarkar, M.S. Khan, Computational modelling of multiphase fluid flow behaviour over a stretching sheet in the presence of nanoparticles, Engineering Science and Technology, an International Journal 23 (3) (2020) 605–617, https://doi.org/10.1016/j.jestch.2019.07.006.

[26] B. Kumar, G.S. Seth, R. Nandkeolyar, A.J. Chamkha, Outlining the impact of induced magnetic field and thermal radiation on magneto-convection flow of dissipative fluid, Int. J. Therm. Sci. 146 (2019) 106101, https://doi.org/10.1016/j.ijthermalsci.2019.106101.

[27] Q. Lou, B. Ali, S.U. Rehman, D. Habib, S. Abdal, N.A. Shah, J.D. Chung, Micropolar dusty fluid: Coriolis force effects on dynamics of MHD rotating fluid when Lorentz force is significant, Mathematics 10 (15) (2022) 2630, https://doi.org/10.3390/math10152630.

[28] L.J. Crane, Flow past a stretching plate, Zeitschrift für angewandte Mathematik und Physik ZAMP 21 (4) (1970) 645–647, https://doi.org/10.1007/BF01587695.

[29] S.S. Ghadikolaei, K. Hosseinzadeh, D.D. Ganji, B. Jafari, Nonlinear thermal radiation effect on magneto Casson nanofluid flow with Joule heating effect over an inclined porous stretching sheet, Case Stud. Therm. Eng. 12 (2018) 176–187, https://doi.org/10.1016/j.csite.2018.04.009.

[30] B.J. Gireesha, M. Umeshaiah, B.C. Prasannakumara, N.S. Shashikumar, M. Archana, Impact of nonlinear thermal radiation on magnetohydrodynamic three-dimensional boundary layer flow of Jeffrey nanofluid over a nonlinearly permeable stretching sheet, Phys. Stat. Mech. Appl. 549 (2020) 124051, https://doi.org/10.1016/j.physa.2019.124051.

[31] A. Ahmed, M. Khan, M. Irfan, J. Ahmed, Transient MHD flow of Maxwell nanofluid subject to non-linear thermal radiation and convective heat transport, Appl. Nanosci. 10 (12) (2020) 5361–5373, https://doi.org/10.1007/s13204-020-01375-1.

[32] Y.M. Chu, S. Aziz, M.I. Khan, S.U. Khan, M. Nazeer, I. Ahmad, I. Tlili, Nonlinear radiative bioconvection flow of Maxwell nanofluid configured by bidirectional oscillatory moving surface with heat generation phenomenon, Phys. Scripta 95 (10) (2020) 105007, https://doi.org/10.1088/1402-4896/abb7a9.

[33] A.K. Gautam, S. Rajput, K. Bhattacharyya, A.K. Pandey, A.J. Chamkha, M. Begum, Comparative study of two non-Newtonian fluids with bioconvective induced MHD flow in presence of multiple slips, heat source/sink and nonlinear thermal radiation, Chemical Engineering Journal Advances 12 (2022) 100365, https://doi.org/10.1016/j.ceja.2022.100365.

[34] M.Y. Ali, S. Reza-E-Rabbi, M.M.H. Rasel, S.F. Ahmmed, Combined impacts of thermoelectric and radiation on hydromagnetic nanofluid flow over a nonlinear stretching sheet, Partial Differential Equations in Applied Mathematics 7 (2023) 100500, https://doi.org/10.1016/j.padiff.2023.100500.

[35] S.R. Logan, The origin and status of the Arrhenius equation, J. Chem. Educ. 59 (4) (1982) 279, https://doi.org/10.1021/ed059p279.

[36] K. Rafiq, M. Irfan, M. Khan, M.S. Anwar, W.A. Khan, Arrhenius activation energy theory in radiative flow of Maxwell nanofluid, Phys. Scripta 96 (4) (2021) 045002, https://doi.org/10.1088/1402-4896/abd903.

[37] X. Zhang, Y. Zhang, Experimental study on enhanced heat transfer and flow performance of magnetic nanofluids under alternating magnetic field, Int. J. Therm. Sci. 164 (2021) 106897, https://doi.org/10.1016/j.ijthermalsci.2021.106897.

[38] S.A. Khan, T. Hayat, M.I. Khan, A. Alsaedi, Salient features of Dufour and Soret effect in radiative MHD flow of viscous fluid by a rotating cone with entropy generation, Int. J. Hydrogen Energy 45 (28) (2020) 14552–14564, https://doi.org/10.1016/j.ijhydene.2020.03.123.
[39] M. Khan, T. Salahuddin, M.Y. Malik, F. Khan, Arrhenius activation in MHD radiative Maxwell nanoliquid flow along with transformed internal energy, The European Physical Journal Plus 134 (5) (2019) 198, https://doi.org/10.1140/epjp/i2019-12563-8.
[40] S.O. Salawu, E.O. Fatunmbi, S.S. Okoya, MHD heat and mass transport of Maxwell Arrhenius kinetic nanofluid flow over stretching surface with nonlinear variable properties, Results in Chemistry 3 (2021) 100125, https://doi.org/10.1016/j.rechem.2021.100125.
[41] F.E. Alsaadi, T. Hayat, M.I. Khan, F.E. Alsaadi, Heat transport and entropy optimization in flow of magneto-Williamson nanomaterial with Arrhenius activation energy, Comput. Methods Progr. Biomed. 183 (2020) 105051, https://doi.org/10.1016/j.cmpb.2019.105051.
[42] M. Ijaz Khan, S. Qayyum, M. Nigar, Y.M. Chu, S. Kadry, Dynamics of Arrhenius activation energy in flow of Carreau fluid subject to Brownian motion diffusion, Numer. Methods Part. Differ. Equ. (2020), https://doi.org/10.1002/num.22615.
[43] S. Reza-E-Rabbi, S.F. Ahmmed, S. Islam, S.M. Arifuzzaman, B.M.J. Rana, M.Y. Ali, M.S. Khan, Characterization of fluid flow and heat transfer of a periodic magnetohydrodynamics nano non-Newtonian liquid with Arrhenius activation energy and nonlinear radiation, Heat Transfer 51 (7) (2022) 6578–6615, https://doi.org/10.1002/htj.22614.
[44] S. Li, K. Raghunath, A. Alfaleh, F. Ali, A. Zaib, M.I. Khan, V. Puneeth, Effects of activation energy and chemical reaction on unsteady MHD dissipative Darcy–Forchheimer squeezed flow of Casson fluid over horizontal channel, Sci. Rep. 13 (1) (2023) 2666, https://doi.org/10.1038/s41598-023-29702-w.
[45] P. Sreedevi, P.S. Reddy, Williamson hybrid nanofluid flow over swirling cylinder with Cattaneo–Christov heat flux and gyrotactic microorganism, Waves Random Complex Media (2021) 1–28.
[46] R. Chandra Sekar Reddy, P.S. Reddy, P. Sreedevi, Impact of the Cattaneo–Christov heat flux on heat and mass transfer analysis of a hybrid nanofluid flow over a vertical cone, Int. J. Ambient Energy 43 (1) (2022) 6919–6931.
[47] P.S. Reddy, P. Sreedevi, S. Venkateswarlu, Impact of modified Fourier's heat flux on the heat transfer of MgO/Fe3O4–Eg-based hybrid nanofluid flow inside a square chamber, Waves Random Complex Media (2022) 1–23.
[48] P.S. Reddy, P. Sreedevi, Effect of Cattaneo–Christov heat flux on heat and mass transfer characteristics of Maxwell hybrid nanofluid flow over stretching/shrinking sheet, Phys. Scripta 96 (12) (2021) 125237.
[49] P.S. Reddy, P. Sreedevi, A.J. Chamkha, Hybrid nanofluid heat and mass transfer characteristics over a stretching/shrinking sheet with slip effects, Journal of Nanofluids 12 (1) (2023) 251–260.
[50] P.S. Reddy, P. Sreedevi, Effect of thermal radiation on heat transfer and entropy generation analysis of MHD hybrid nanofluid inside a square cavity, Waves Random Complex Media (2022) 1–33.
[51] M. Santhi, K.V. Suryanarayana Rao, P. Sudarsana Reddy, P. Sreedevi, Heat and mass transfer characteristics of radiative hybrid nanofluid flow over a stretching sheet with chemical reaction, Heat transfer 50 (3) (2021) 2929–2949.
[52] B. Prabhavathi, P.S. Reddy, R.B. Vijaya, A. Chamkha, MHD boundary layer heat and mass transfer flow over a vertical cone embedded in porous media filled with Al2O3-water and Cu-water nanofluid, Journal of Nanofluids 6 (5) (2017) 883–891.
[53] A. Zeeshan, O.U. Mehmood, F. Mabood, F. Alzahrani, Numerical analysis of hydromagnetic transport of Casson nanofluid over permeable linearly stretched cylinder with Arrhenius activation energy, Int. Commun. Heat Mass Tran. 130 (2022) 105736.
[54] M.B. Arain, M.M. Bhatti, A. Zeeshan, F.S. Alzahrani, Bioconvection reiner-rivlin nanofluid flow between rotating circular plates with induced magnetic effects, activation energy and squeezing phenomena, Mathematics 9 (17) (2021) 2139.
[55] Z. Ali, A. Zeeshan, M.M. Bhatti, A. Hobiny, T. Saeed, Insight into the dynamics of Oldroyd-B fluid over an upper horizontal surface of a paraboloid of revolution subject to chemical reaction dependent on the first-order activation energy, Arabian J. Sci. Eng. 46 (2021) 6039–6048.
[56] R. Kumar, J. Singh, R. Mehta, D. Kumar, D. Baleanu, Analysis of the impact of thermal radiation and velocity slip on the melting of magnetic hydrodynamic micropolar fluid-flow over an exponentially stretching sheet, Therm. Sci. 27 (Spec. issue 1) (2023) 311–322, https://doi.org/10.2298/TSCI23S1311K.
[57] M.M. Biswal, K. Swain, G.C. Dash, K. Ojha, Study of radiative magneto-non-Newtonian fluid flow over a nonlinearly elongating sheet with Soret and Dufour effects, Numer. Heat Tran., Part A: Applications 83 (4) (2023) 331–342, https://doi.org/10.1080/10407782.2022.2091379.
[58] I.V. Miroshnichenko, M.A. Sheremet, Influence of thermal radiation on heat transfer through a hollow block, Journal of Applied and Computational Mechanics 9 (2) (2023) 419–429, https://doi.org/10.22055/JACM.2022.41759.3805.
[59] K.G.R. Deepthi, S. Kavitha, V.V. Murthy, Steady 3-D magneto hydrodynamics-casson moving fluid across a porous sheet as it is being linearly stretched out thermal radiation and Prandtl number: FEM approach, Journal of Nanofluids 12 (5) (2023) 1454–1461, https://doi.org/10.1166/jon.2023.2031.
[60] Z. Sabir, A. Ayub, J.L. Guirao, S. Bhatti, S.Z.H. Shah, The effects of activation energy and thermophoretic diffusion of nanoparticles on steady micropolar fluid along with Brownian motion, Adv. Mater. Sci. Eng. (2020), https://doi.org/10.1155/2020/2010568, 2020.